Inorganic Chemistry

Article

pubs.acs.org/IC

Exploring the Coordination Chemistry of 3,3′-Di(picolinamoyl)-2,2′-bipyridine: One Ligand, Multiple Nuclearities

Nicholas J. Hurley,[†] John J. Hayward,[†] Jeremy M. Rawson,[‡] Mark Murrie,[§] and Melanie Pilkington*,[†]

[†]Department of Chemistry, Brock University, 500 Glenridge Ave, St Catharines, Ontario, Canada L2S 3A1

[‡]Department of Chemistry and Biochemistry, University of Windsor, 401 Sunset Ave., Windsor, Ontario, Canada N9B 3P4

[§]School of Chemistry, Joseph Black Building, University Ave, Glasgow, Lanarkshire G12 8QQ, United Kingdom

Supporting Information

ABSTRACT: The syntheses, structures, and magnetic properties of three new coordination complexes, tetranuclear $[Zn_2L^3(OAc)(OMe)]_2{\cdot}3MeOH{\cdot}H_2O$ (**3**), trinuclear $[Ni_3(L^3)_3]{\cdot}6H_2O$ (**4**), and a 1-D chain $\{[Cu_2L^3(OAc)_2]_2{\cdot}H_2O\}_n$ (**6**), of a polydentate, doubly deprotonated, 3,3′-disubstituted bipyridine ligand $[L^3]^{2-}$ are reported. The X-ray crystal structures demonstrate that the ditopic ligand provides a flexible N_3 donor set for transition metal ions where each binding pocket shifts from *fac* to intermediate *fac*/*mer* to the *mer* isomer affording a Ni_3 triangle, a Zn_4 tetramer, and a 1-D Cu(II) polymer, respectively. This variation in coordination preference is rationalized with the aim of designing future ligands with controlled coordination modes. Magnetic susceptibility studies on **4** reveal it belongs to the rare family of ferromagnetically coupled $[Ni_3]$ clusters. In contrast, magnetic studies of the 1-D chain **6** reveal weak antiferromagnetic interactions due to the poor orbital overlap of the singly occupied Cu(II) $d_{x^2-y^2}$ orbitals with the one-atom bridge that connects them along the Jahn−Teller distortion axis.

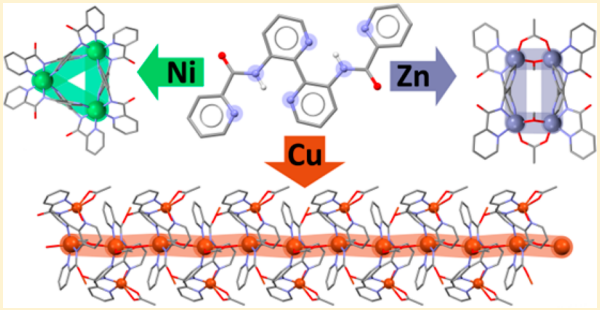

INTRODUCTION

The spatial arrangement of atoms and molecules in the solid state is integral to their materials properties, and extensive research has been invested in the rational design of supramolecular architectures such as clusters and chains.[1] Within the field of supramolecular chemistry the preferred 4-, 5-, or 6-coordinate geometry of transition metal ions coupled with control of ligand denticity has been implemented to design elegant topologies including molecular squares, tetrahedra, knots, and both double and triple helices, *inter alia*.[2] In these systems control of both the coordination geometry of the metal center and ligand topology provides a diverse core upon which functional materials can be built, with the properties of the metal ions strongly influenced by the chemical nature and denticity of the organic ligands employed.[3] However, the behavior becomes more complex for ions where there is no strong crystal field stabilization energy to favor a specific local geometry at the templating center. For example, spherically symmetric charge distributions in high spin d^5 Mn(II) and d^{10} Zn(II) ions favor both tetrahedral and octahedral geometries, whereas d^3 and low spin d^6 configurations exhibit a strong preference for octahedral coordination. The outcome of reactions of metal centers which offer more flexible coordination environments therefore provides a particular challenge, especially in the presence of flexible polydentate ligands. However, the versatility of both the metal center and polydentate ligand can lead to equally beautiful structural topologies.

2,2′-Bipyridine[4] (bipy) is arguably the most common chelating ligand exploited in the field of coordination chemistry with over 7000 complexes of this ligand deposited in the Cambridge Structural Database (CSD) in addition to numerous reports describing closely related derivatives. Substitutions at the 4-, 5-, and 6-positions of the pyridine rings are well-known and are commonly performed to modulate the chemical and physical properties of the corresponding complexes, which are widely applied in diverse fields such as catalysis,[5] optoelectronics,[6] and macromolecular chemistry.[7] Distinctly less well-studied are substitutions at the 3,3′-positions; chelation of the bipyridine rings to a metal center leads to compression of the 3- and 3′-positions, and hence bulky substituents can inhibit the usual chelated binding mode observed in their 2,2′-bipyridine counterparts. However, in recent years a wide variety of substituents have been introduced into these positions which still leads to N,N′-chelation, such as 3,3′-dimethyl,[8a] 3,3′-dinitro,[8b] 3,3′-dicarboxylate,[8c] 3,3′-diester,[8d] 3,3′-dihydroxy,[8e] and 3,3′-diarylphosphoryl[8f]-2,2′-bipyridine derivatives, as well as 3,3′-diamino-2,2′-bipyridine, L^1.[9] The introduction of functionality capable of coordinating to metals have also afforded 3,3′-dihydroxy[10] and 3,3′-dicarboxylate derivatives.[11] To date the coordination chemistry of the dicarboxylate derivatives[7c] has been the most extensively studied affording 1-D chain complexes assembled from N,N′-chelation and O-

Received: May 27, 2014
Published: July 29, 2014

dx.doi.org/10.1021/ic501224q | *Inorg. Chem.* 2014, 53, 8610−8623

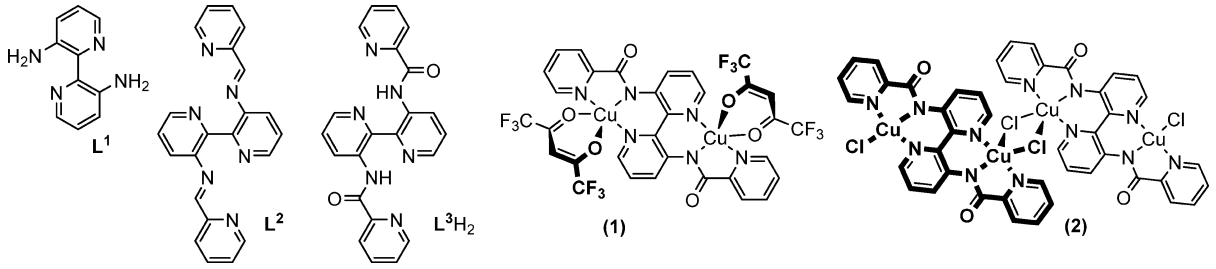

Figure 1. 3,3′-Diamino-2,2′-bipyridine $\mathbf{L}^1$, the Schiff-base *bis*-imine ligand $\mathbf{L}^2$, *bis*-picolinoylamide derivative $\mathbf{L}^3H_2$, and previously reported copper complexes **1** and **2**.[17]

coordination motifs,[12] though structures which coordinate only through the anionic side chain are also now well established.[13] Although not as widely exploited as bipy, a second versatile family of ligands are the pyridine carboxamides.[14] These contain both pyridine nitrogen donor atoms as well as amide functional groups that can coordinate either via the carbonyl oxygen when neutral or via the amide nitrogen when deprotonated; additionally, the ability of both heteroatoms in the functional group to act as donors also means that the amide group can act as a bridging group to bind to multiple metal centers. Complexes of these ligands have been used in a variety of catalytic applications[15] and have been shown to stabilize high-oxidation state metals such as Ni(IV).[18]

As part of our research program directed toward exploiting bipyridyl ligands for the preparation of new classes of polydentate ligands,[9,16−18] we previously reported the synthesis and coordination chemistry of 3,3′-diamino-2,2′-bipyridine $\mathbf{L}^1$, where the preferred mode of chelation can be tuned by varying the pH of the reaction.[9] In recent years, additional binding sites have been introduced into this core framework in the form of 2-pyridyl imines ($\mathbf{L}^2$)[16] and amide substituents ($\mathbf{L}^3$).[17] The coordination of $\mathbf{L}^2$ to a Co(II) metal ion resulted in a substantial rearrangement sequence affording a mononuclear quaterpyridine-like complex which was attributed to the high susceptibility of the imine linkage to nucleophilic attack. In contrast, the amide ligand [$\mathbf{L}^3$] remains intact upon coordination of transition metal ions and we have reported the structural and magnetic properties of two copper complexes, both of which are chelated in a *mer* fashion; a dinuclear monomer, (**1**), with hexafluoroacetylacetonate (hfac) counterions and a tetranuclear dimeric structure, (**2**), with bridging chloride ions (Figure 1).[17]

Intrigued by the ability of $\mathbf{L}^3$ to act as a scaffold for diverse structural motifs we investigated further its coordination chemistry with first row transition metal ions and report herein three new structural topologies comprising a Zn(II) tetranuclear dimer (**3**), two [Ni_3] triangles (**4** and **5**), and a 1-D Cu(II) chain (**6**), highlighting the versatility of this ligand to stabilize a range of interesting structural topologies.

EXPERIMENTAL SECTION

General Considerations. All experiments were performed under a nitrogen atmosphere unless stated otherwise. Dry solvents were obtained from a Puresolve PS MD-4 solvent purification system. 3,3′-Diamino-2,2′-bipyridine $\mathbf{L}^1$ was prepared as previously reported;[9] $\mathbf{L}^3H_2$ was prepared by a modification of the literature method.[17] All chemicals were commercially available and used as received, unless otherwise stated.

Physical Measurements. NMR spectra were recorded on a Bruker Avance AV 600 Digital NMR spectrometer with a 14.1 T Ultrashield Plus magnet. Samples for IR were pressed as KBr pellets and their spectra were recorded using a ThermoMattson RS-1 FT-IR. EI and FAB mass spectra were obtained using a Kratos Concept 1S High Resolution E/B mass spectrometer. Samples for elemental analysis were submitted to Atlantic Microlab. All samples were predried under vacuum before CHN analysis.

Synthesis. *N,N′-([2,2′-Bipyridine]-3,3′-diyl)dipicolinamide, L^3H_2.*[17] 3,3′-Diamino-2,2′-bipyridine $\mathbf{L}^1$ (1.17) (0.466 g, 2.50 mmol) was dissolved in freshly distilled pyridine (3.5 mL). To this was added picolinic acid (0.650 g, 5.28 mmol) in one portion. This mixture was allowed to stir at 45 °C for 45 min after which time triphenylphosphite (1.31 mL, 5.00 mmol) was added via syringe over 5 min and the solution heated to 95 °C for 4 h. The resulting thick slurry was allowed to cool to room temperature and filtered. The residue was washed with water (3 × 15 mL), acetone (3 × 15 mL), and diethyl ether (20 mL) to yield $\mathbf{L}^3H_2$ as a light beige solid (0.90 g, 92%). The analytical data is consistent with literature values.[17]

[Please note that the formula used for the complexes in each section (**3**−**6**) is calculated based on the CHN data of the pre-dried solids which as expected differs from the formula determined from the X-ray diffraction experiments.] [$Zn_2\mathbf{L}^3(OAc)(OMe)]_2{\cdot}3MeOH{\cdot}H_2O$, (**3**).

2,2′-Bipyridine-3,3′-(2-pyridinecarboxamide) ($\mathbf{L}^3H_2$) (50.0 mg, 0.13 mmol) was dissolved in DCM (15 mL) and triethylamine (0.036 mL, 0.26 mmol). To this solution was added $Zn(OAc)_2{\cdot}2H_2O$ (58.2 mg, 0.27 mmol) in MeOH (5 mL). The resulting yellow solution was stirred at room temperature for 15 h. Removal of the solvents under reduced pressure afforded a beige solid which was washed with water (15 mL), filtered, then washed with Et_2O (15 mL), and finally dried under vacuum to yield **3** as a beige powder (46 mg, 60%). MS (FAB) m/z = 1042 $[Zn_3(\mathbf{L}^3)_2OAc]^+$ (3.9%), 919 $[Zn_2(\mathbf{L}^3)_2]^+$ (3.2%), 676 $[Zn_2\mathbf{L}^3(OAc)_2(OMe)]^+$ (16%). FT-IR (KBr, cm^{-1}): ν_{max} = 3403, 3075, 2983, 2682, 2489, 2360, 1637, 1600, 1417, 1334, 1297, 1160, 995, 802, 757, 657. UV−vis (DCM, nm): λ_{max} = 230 (ε = 29 980 $M^{-1}{\cdot}cm^{-1}$), 257 (ε = 26 140 $M^{-1}{\cdot}cm^{-1}$), 309 (ε = 22 760 $M^{-1}{\cdot}cm^{-1}$), 341 (ε = 19 080 $M^{-1}{\cdot}cm^{-1}$). Elemental analysis: Calculated for $Zn_4C_{53}H_{52}N_{12}O_{14}$: C 47.34%, H 4.05%, N 12.50%; found: C 47.02%, H 3.79%, N 12.34%.

$[Ni_3(\mathbf{L}^3)_3]{\cdot}6H_2O$, (4). 2,2′-Bipyridine-3,3′-(2-pyridinecarboxamide) ($\mathbf{L}^3H_2$, 50.0 mg, 0.13 mmol) was dissolved in DCM (15 mL) and triethylamine (0.036 mL, 0.26 mmol). To this solution was added $NiCl_2{\cdot}6H_2O$ (63.0 mg, 0.27 mmol) dissolved in methanol (5 mL). The resulting yellow solution was stirred at room temperature for 15 h. Removal of the solvents under vacuum afforded a yellow solid which was washed with water (15 mL), filtered, then washed with diethyl ether (15 mL), and finally dried under vacuum to yield complex **4** as a yellow/orange solid (46 mg, 75%). MS (FAB) m/z = 964 $[Ni_3(\mathbf{L}^3)_2]^+$ (10%), 511 $[Ni_2\mathbf{L}^3]^+$ (6.1%), 452 $[Ni\mathbf{L}^3]^+$ (51%). FT-IR (KBr, cm^{-1}): ν_{max} = 3403, 3070, 2946, 2356, 1614, 1563, 1515, 1436, 1384, 1294, 1226, 1118, 1087, 1018, 904, 804, 740, 694, 638. UV−vis (DCM, nm): λ_{max} = 229 (ε = 34 640 $M^{-1}{\cdot}cm^{-1}$), 262 (ε = 24 120 $M^{-1}{\cdot}cm^{-1}$), 331 (ε = 12 960 $M^{-1}{\cdot}cm^{-1}$). Elemental analysis: Calculated for $C_{66}H_{42}N_{18}Ni_3O_6{\cdot}6H_2O$: C 54.02%, H 3.71%, N 17.18%; found: C 53.79%, H 3.67%, N 17.15%.

$[Ni_3(\mathbf{L}^3)_3]{\cdot}4H_2O$, (5). 2,2′-Bipyridine-3,3′-(2-pyridinecarboxamide) ($\mathbf{L}^3H_2$) (50.0 mg, 0.13 mmol) was dissolved in DCM (15 mL) and triethylamine (0.036 mL, 0.26 mmol). To this solution was added $Ni(OAc)_2{\cdot}4H_2O$ (66.0 mg, 0.27 mmol) dissolved in methanol (5 mL).

dx.doi.org/10.1021/ic501224q | *Inorg. Chem.* 2014, 53, 8610−8623

Table 1. Summary of Crystallographic Data for L^3H_2 and Coordination Complexes 3−6

	L^3H_2	3	4	5	6
chemical formula	$C_{22}H_{16}N_6O_2$	$Zn_4C_{50}H_{40}N_{12}O_{10}$	$C_{75}H_{86}N_{18}Ni_3O_{19}$	$C_{66}H_{66}N_{18}O_{18}Ni_3$	$Cu_2C_{26}H_{20}N_6O_7$
formula mass	396.41	1230.45	1719.74	1575.49	655.56
crystal system	monoclinic	orthorhombic	trigonal	trigonal	monoclinic
a/Å	14.1606(13)	17.1472(8)	23.3442(16)	23.843(3)	31.202(2)
b/Å	3.9083(3)	22.4405(10)	23.3442(16)	23.843(3)	9.1176(6)
c/Å	16.1931(13)	16.7592(7)	24.987(4)	20.481(7)	21.4203(14)
α/°	90	90	90	90	90
β/°	94.593(4)	90	90	90	123.052(3)
γ/°	90	90	120	120	90
unit cell volume/Å^3	893.31(3)	6448.8(5)	11792.(4)	10083(3)	5107.7(6)
temp/K	150(2)	150(2)	150(2)	150(2)	150(2)
space group	$P2_1/c$	$Cmca$	$R\bar{3}c$	$R\bar{3}c$	$C2/c$
no. of formula units per unit cell, Z	2	4	6	6	8
No. of reflections measured	10 625	55 753	111 604	82 417	102 462
no. of independent reflections	1163	3779	2582	2327	6375
R_{int}	0.0472	0.0343	0.0469	0.0775	0.0643
final R_1 values ($I > 2\sigma(I)$)	0.0719	0.0496	0.0868	0.0605	0.0287
final $wR(F^2)$ values ($I > 2\sigma(I)$)	0.1918	0.2435	0.2177	0.1603	0.0736
final R_1 values (all data)	0.0901	0.0532	0.1225	0.0958	0.0388
final $wR(F^2)$ values (all data)	0.2122	0.2523	0.2841	0.1971	0.0819

The resulting yellow solution was stirred at room temperature for 15 h. Removal of the solvents under vacuum afforded a yellow solid which was washed with water (15 mL), filtered, washed with diethyl ether (15 mL), and finally dried under vacuum to yield complex **5** as a yellow powder (40 mg, 65%). MS (FAB) m/z = 964 $[Ni_3(\mathbf{L^3})_2]^+$ (7.2%), 510 $[Ni_2\mathbf{L^3}]^+$ (12%), 453 $[Ni\mathbf{L^3}]^+$ (11%). FT-IR (KBr, cm^{-1}): ν_{max} = 3403, 3068, 2985, 2686, 2493, 2360, 1860, 1612, 1589, 1556, 1438, 1411, 1346, 1292, 1089, 1020, 910, 804, 761, 694. UV−vis (DCM, nm): λ_{max} = 230 (ε = 34 040 M^{-1}·cm^{-1}), 262 (ε = 23 800 M^{-1}·cm^{-1}), 331 (ε = 12 720 M^{-1}·cm^{-1}). Elemental Analysis: Calculated for $C_{66}H_{42}N_{18}Ni_3O_6$·$4H_2O$: C 55.38%, H 3.52%, N 17.61%; found: C 55.54%, H 3.67%, N 17.38%.

{[$Cu_2\mathbf{L^3}(OAc)_2$]·H_2O}$_n$ (**6**). 2,2′-Bipyridine-3,3′-(2-pyridinecarboxamide) ($\mathbf{L^3}H_2$, 50.0 mg, 0.13 mmol) was dissolved in DCM (15 mL) and triethylamine (0.036 mL, 0.26 mmol). To this solution was added $[Cu_2(OAc)_4·(H_2O)_2]$ (85 mg, 0.25 mmol) dissolved in methanol (5 mL). The resulting green solution was stirred at room temperature for 15 h. Removal of the solvents under vacuum afforded a green oily solid which was washed with water (15 mL), filtered, then washed with diethyl ether (15 mL), and finally dried under vacuum to yield **6** as a green crystalline powder (62 mg, 77%). MS (FAB) m/z = 642 $[Cu_2\mathbf{L^3}(OAc)_2]^+$ (11%), 579 $[Cu_2\mathbf{L^3}(OAc)]^+$ (59%), 520 $[Cu_2\mathbf{L^3}]^+$ (3%). 8FT-IR (KBr, cm^{-1}): ν_{max} = 3072, 2981, 2360, 1637, 1598, 1569, 1421, 1344, 1301, 1226, 1155, 1022, 954, 858, 808, 757, 688, 649. UV−vis (DCM, nm): λ_{max} = 228 (ε = 26 780 M^{-1}·cm^{-1}), 256 (ε = 25 220 M^{-1}·cm^{-1}), 320 (ε = 12 320 M^{-1}·cm^{-1}), 363 (ε = 10 160 M^{-1}·cm^{-1}), 667 (ε = 1234 M^{-1}·cm^{-1}). Elemental Analysis: Calculated for $Cu_2C_{26}H_{22}N_6O_7$: C 47.49%, H 3.37%, N 12.78%; found: C 47.39%, H 3.67%, N 12.97%.

X-ray Crystallography. Single crystals of $\mathbf{L^3}H_2$ and complexes **3**−**6** were mounted on a cryoloop with paratone oil and examined on a Bruker APEX-II CCD diffractometer equipped with an Oxford Cryostream low temperature device. Data were measured at 150(2) K using graphite-monochromated Mo-Kα radiation (λ= 0.71073 Å) and Bruker APEX-II software.[19] Final cell constants were determined from full least-squares refinement of all observed reflections. The data were corrected for absorption (Bruker-SADABS).[20] For all compounds, the structures were solved by direct methods with SHELXS[21] and refined by full-matrix least-squares on F^2 with SHELXL.[21] Hydrogen atoms were placed in calculated positions and refined as riding atoms using default parameters. Reflection data for **3** contained residual electron density peaks consistent with eight disordered methanol molecules and three disordered water molecules which could not be adequately modeled and hence was removed using the SQUEEZE routine within PLATON.[22] This omitted solvent is not included in the molecular formula for **3**. For complexes **4** and **5** , we were unable to locate the H atoms for the solvent water molecules. Thus, in complex **4** there is a discrepancy of 8H per formula unit or 48H per unit cell, whereas for complex **5**, there is a discrepancy of 24H per formula unit or 144H per unit cell. Crystallographic data for ligand $\mathbf{L^3}H_2$ and complexes **3**−**6** are summarized in Table 1. All five structures have been deposited with the CCDC (deposition numbers CCD 999759−999763).

EPR Data. A room temperature EPR spectrum of a polycrystalline sample of (**6**) mounted in a quartz tube was measured on a Bruker Elexsys E-580 X-band EPR spectrometer with a microwave frequency of 9.8705 GHz and 2 G modulation. A simulation was made using PIP (M. Nilges, Ilinois EPR Research Centre) via a Windows interface.[23] An initial cubic (isotropic) simulation reproduced the broad features and initial estimates of g-values, but failed to reflect some anisotropy in the line shape evident from differences between observed and simulated profiles. The symmetry was lowered to axial and provided a more satisfactory fit to the experimental data.

Magnetic Susceptibility Data. Variable temperature dc magnetic susceptibility data were collected on single crystals of **4** and **6** on a Quantum Design MPMS SQUID magnetometer in an applied field of 0.1 T from 2−300 K. Pascal's constants were used to estimate the diamagnetic corrections, which were subtracted from the experimental susceptibilities to give the molar paramagnetic susceptibilities (χ_M). Ac susceptibility data for **4** were measured in zero field with an oscillating 3 Oe field in the frequency region 1−1270 Hz in the temperature range 1.8−10 K.

Computational studies. Unrestricted density functional theory (UDFT) calculations were undertaken on **4** to probe the magnetic exchange interactions within the complex. The single point energy and expectation value ($\langle S^2 \rangle$) were calculated for both the S = 3 and S = 1 spin states using an initial guess in which the spin (S = 1) and formal charge (+2) on each Ni were explicitly specified (and balanced with a −2 charge on the ligand fragments) using the &atomic command within Jaguar.[24] The 1SCF calculations employed the LACVP**++ basis set (which consists of the Pople 6-31G basis set[25] for lighter atoms and the LANL2DZ basis set[26] for heavier atoms) and the B3LYP[27] functional.

RESULTS AND DISCUSSION

While the ligand $\mathbf{L^3}H_2$ has been previously reported,[17] its molecular structure has not yet been characterized by X-ray

dx.doi.org/10.1021/ic501224q | Inorg. Chem. 2014, 53, 8610−8623

crystallography. Single crystals of L^3H_2 were grown via slow evaporation of a saturated dichloromethane solution at room temperature affording colorless plates after 1 week. The ligand crystallizes in the monoclinic space group $P2_1/c$ with half a molecule in the asymmetric unit and two molecules in the unit cell. The molecular structure of the ligand together with the appropriate labeling scheme is shown in Figure 2. Tables of

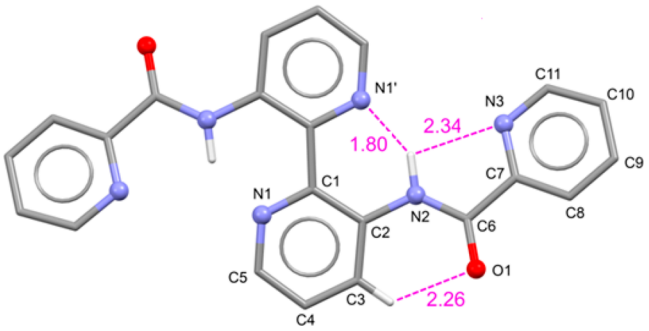

Figure 2. Molecular structure of L^3H_2, highlighting the bifurcated intramolecular H-bond stabilizing the *trans* configuration of the ligand. Hydrogen atoms not involved in H-bonding are omitted for clarity. Distances are given in Å.

bond lengths and angles for L^3H_2 can be found in the Supporting Information (S-1). The amide groups are effectively coplanar with the pendant pyridyl moieties, which are twisted by an angle of 21.2° with respect to the best plane of the 2,2′-bipyridine backbone. The 2,2′-bipyridine core adopts an *s-trans* configuration with respect to the coplanar pyridine rings, stabilized by hydrogen bonding to the N(2) hydrogen atom. The N(2) hydrogen atom is bifurcated with a short interaction to the bipyridine nitrogen (N(2)−H···N(1′) = 1.80 Å; ∠N(2)−H(2)−N(1)′ = 145°) and a longer hydrogen bond to the terminal pyridine nitrogen atom (N(2)−H···N(3) = 2.34 Å; ∠N(2)−H(2)−N(3) = 102°), Figure 2. Interestingly, the H-bond from the amide NH to the pyridyl N is ca. 0.15 Å shorter than the corresponding N−H···N bond length of 1.95 Å in the previously reported 3,3′-diamino-2,2′-bipyridine ligand,[9] consistent with a more acidic amide proton due to delocalization of its N atom with the carbonyl group.

The carbonyl O(1) atom is involved in an intramolecular hydrogen bond to the adjacent aromatic H(3) proton such that C(3)-H···O(1) = 2.26 Å; ∠C(3)−H(3)−O(1) = 120°). There are no significant intermolecular hydrogen bonding interactions; instead the crystal packing of L^3H_2 reveals a herringbone arrangement of molecules stabilized by C−H···π interactions, (Figure 3), reminiscent of the crystal packing motifs commonly observed in neutral aromatic molecules.[28] In this respect, each molecule forms a set of contacts to four other molecules in a symmetrical fashion; the closest C−H···π bonds are C(3)···H−C(11′) = 3.72 Å and C(5)···H−C(5′) = 3.46 Å from the centroid of the ring.

Coordination Chemistry of L^3H_2 with First Row Transition Metals. Coordination chemistry studies were undertaken employing a range of first row transition metal salts with chloride or acetate counterions. In a typical experiment, 2.1 equiv of the metal salt were reacted together with one equivalent of ligand L^3H_2 in a 3:1 mixture of DCM:MeOH (Scheme 1). Lewis acidic transition metal cations can promote the deprotonation of amides; as was previously reported for L^3H_2 with Cu(II) salts.[17] However, in order to

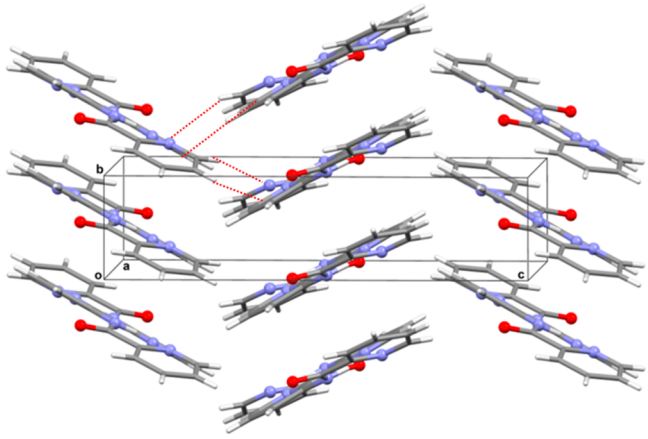

Figure 3. Packing diagram showing the herringbone arrangement of L^3H_2 molecules running along the crystallographic *a*-axis. Intermolecular C−H···π interactions between neighboring stacks are shown as red dashed lines.

Scheme 1. Coordination Chemistry of $[L^3]^{2-}$ with Divalent Transition Metal Salts

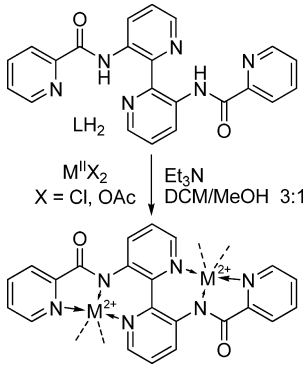

promote deprotonation and generate the anionic form of the ligand, $[L^3]^{2-}$, 2 equiv of triethylamine were also added; therefore, in all cases herein the ditopic ligand is doubly deprotonated and coordinates as shown in Scheme 1. Studies of the coordination chemistry of $[L^3]^{2-}$ with Mn(II) and Co(II) salts were also undertaken. With chloride salts the CHN microanalysis data was consistent with the formation of a 2:1 metal to ligand complex, whereas the acetate salts afforded 3:1 complexes. Unfortunately, single crystals of these complexes could not be obtained and these reactions will not be discussed further.

Reaction of $[L^3]^{2-}$ with zinc acetate afforded the tetranuclear complex **3** as a beige crystalline solid in 60% yield. The CHN data are an excellent fit for $[Zn_2L^3(OAc)(OMe)]_2{\cdot}3MeOH{\cdot}H_2O$. The UV−vis spectrum in dichloromethane shows three absorption bands centered at λ_{max} = 257, 309, and 341 nm assigned to ligand-based $\pi-\pi^*$ and n−π^* electronic transitions. Unfortunately, the limited solubility of the complex in conventional organic solvents precluded the observation of Laporte forbidden *d-d* transitions. The FAB MS spectrum of **3** shows peaks at m/z = 1042, 919, and 676 corresponding to $[Zn_3(L^3)_2(OAc)]^+$, $[Zn_2(L^3)_2]^+$, and $[Zn_2L^3(OAc)_2(OMe)]^+$ ions, respectively. Interestingly, the $\nu_{C=O}$ stretch at 1674 cm^{-1} in the IR spectrum is not shifted with respect to the free ligand hinting that the amide bond in the structure is not particularly delocalized in the coordination complex. Additional bands at ν = 1562 and 1513 cm^{-1} are assigned to asymmetric stretching

dx.doi.org/10.1021/ic501224q | Inorg. Chem. 2014, 53, 8610−8623

C−O modes, while the bands at ν = 1463 and 1432 cm^{-1} are assigned to symmetric stretches of the acetate functionality and are consistent with a bidentate mode of chelation.[29]

Single crystals of **3** were obtained via the slow evaporation of a 1:1 DCM:MeOH solution and were characterized by X-ray diffraction. The complex crystallizes in the orthorhombic space group *Cmca* with a quarter of a molecule in the asymmetric unit. The molecular structure reveals that **3** comprises four Zn(II) ions, two deprotonated ditopic carboxamide ligands $[L^3]^{2-}$, two bridging μ_2-methoxides, and two bridging 1,3-μ_2-acetate anions. The topology can be considered as a rectangular array of Zn(II) ions with a pair of $[L^3]^{2-}$ ligands bridging opposite edges of the rectangle and the acetate and methoxide bridging the other two edges (Figure 4). Each pocket of the carboxamide ligand chelates in the expected bis-tridentate fashion through the bipyridine (N3′), amide (N2) and terminal pyridine (N1) nitrogen atoms, while the carbonyl oxygen (O1) remains uncoordinated. Two additional oxygen atoms (O3) and (O4), from an acetate group and a methoxide ion respectively, complete the five-coordinate N_3O_2 geometry around the Zn(II) ions and balance the overall charge of the complex. The coordination geometry around the crystallographically unique Zn(II) center is best described as being intermediate between trigonal bipyramidal and square pyramidal; the distortion parameter τ,[30] is calculated to be 0.48 ($\tau = (\theta_1 - \theta_2)/60$; in which the largest angles in the coordination sphere are designated θ_1 and θ_2 and τ = 0 for square pyramidal and τ = 1 for trigonal bipyramidal).

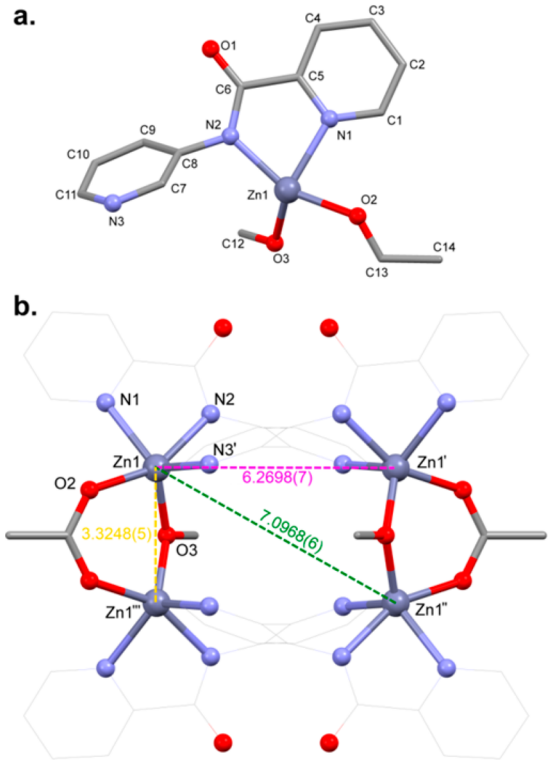

Figure 4. (a) Asymmetric unit of the zinc complex **3** showing the numbering scheme. (b) Crystal structure of the tetranuclear dimer highlighting the internuclear Zn···Zn distances. The carbon atoms of L^3 are shown in wireframe. Hydrogen atoms are removed for clarity; distances are in Å. Symmetry transformations used to generate equivalent atoms: Zn1′: x, 1 − y, −z; Zn1″: 1 − x, 1 − y, −z ; Zn1‴: 1 − x, y, z.

The angles associated with the ZnN_3 fragment are 76.59(11), 83.15(9), and 125.47(9)° respectively with the N atoms adopting two equatorial and one axial position enforcing a *pseudo-fac* arrangement. The torsion angle between the best planes of the bipyridine backbone is 45°; the terminal pyridine lies at 54° to the bipyridine ring it is directly attached to and at 78° to the more remote bipy pyridine ring. The amide N remains in conjugation with the terminal pyridyl ring with an angle of 4° between the best planes of the two groups, while the torsion angle of 58° between the best planes of the amide and the pyridine of the bipy backbone suggests that the conjugation is lost. There is a short distance between the Zn(II) ions across the oxygen bridge of 3.3248(5) Å, while the distance between the two centers bound to the same ligand is significantly longer at 6.2698(7) Å. Selected bond lengths and angles for **3** are presented in Table 2; the pyridyl donor atoms, N(1) and N(3) form longer contacts to the metal ion than the deprotonated amide nitrogen N(2), consistent with the general trend seen in the literature.[14b]

The carbonyl group forms a C−H···O hydrogen bond between O(1) and the hydrogen attached to C(9) of a bipyridyl ring (Figure 5a). With each asymmetric unit acting as a C−H bond donor and a C═O hydrogen bond acceptor, the 4-fold symmetry generates eight such symmetry equivalent contacts per molecule affording a two-dimensional array in the crystallographic *ac*-plane (Figure 5b). Disordered solvent atoms occupy the large solvent-accessible void (Figure 6) that occupies 27% of the unit cell (1763 $Å^3$).

Reaction of ligand $[L^3]^{2-}$ with 2.1 equiv of $NiCl_2$ was carried out following the general procedure described in Scheme 1. Complex **4** was isolated as a yellow/orange solid in 75% yield. Despite the 2:1 reaction, the CHN data was an excellent fit for a 1:1 complex of stoichiometry $[Ni_3(L^3)_3]\cdot 6H_2O$. The IR spectrum of **4** exhibits a $\nu_{C=O}$ stretch at 1614 cm^{-1} which is

Table 2. Selected Bond Lengths and Angles for the Zinc Complex 3[a]

atoms	bond [Å]	atoms	bond [Å]
Zn(1)−N(1)	2.164(3)	Zn(1)−O(2)	2.033(2)
Zn(1)−N(2)	2.031(2)	Zn(1)−O(3)	1.949(2)
Zn(1)−N(3′)	2.173(3)		
atoms	angle [deg]	atoms	angle [deg]
O(3)−Zn(1)−N(2)	106.50(12)	O(2)−Zn(1)−N(1)	84.24(9)
O(3)−Zn(1)−O(2)	98.01(11)	O(3)−Zn(1)−N(3)#1	111.29(12)
N(2)−Zn(1)−O(2)	154.46(9)	N(2)−Zn(1)−N(3)#1	83.15(9)
O(3)−Zn(1)−N(1)	122.88(12)	O(2)−Zn(1)−N(3)#1	94.72(9)
N(2)−Zn(1)−N(1)	76.59(11)	N(1)−Zn(1)−N(3)#1	125.47(9)

[a]Symmetry transformations used to generate equivalent atoms: #1: x, 1 − y, −z.

dx.doi.org/10.1021/ic501224q | Inorg. Chem. 2014, 53, 8610−8623

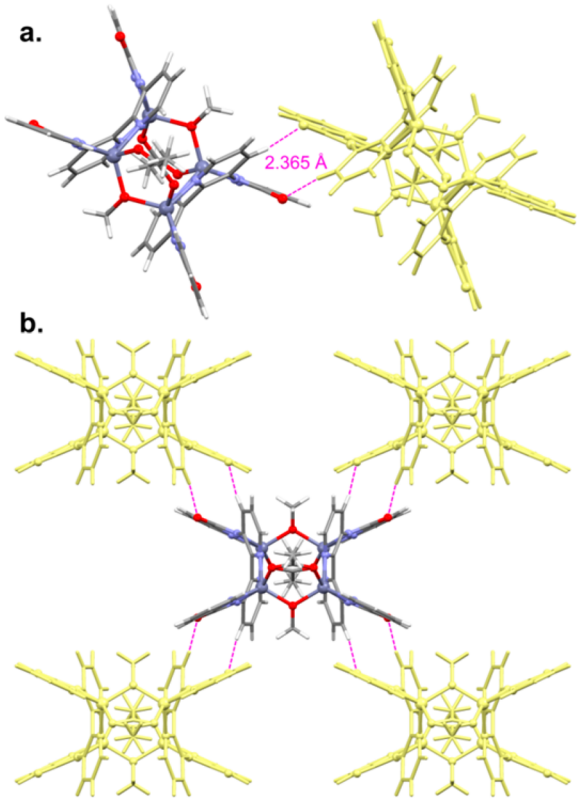

Figure 5. (a) Intermolecular ^{Ar}C−H···O hydrogen bonds between the amide oxygen and the aryl C−H in the 4 position on the bipyridine backbone of **3**; (b) View along the crystallographic *b*-axis showing the interactions propagating through the crystallographic *ac*-plane.

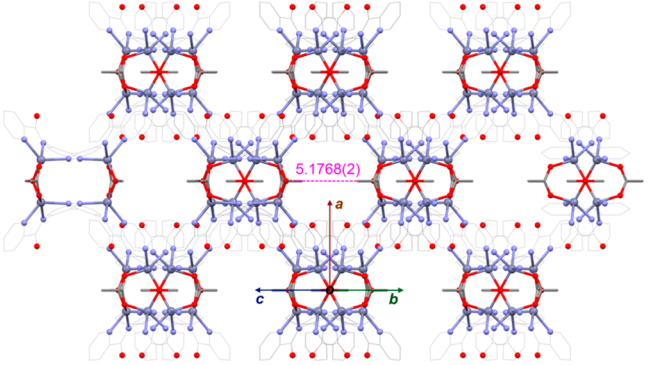

Figure 6. Crystal packing of **3**; view along the crystallographic *bc* intersect displaying the solvent accessible cavities in the crystal structure. The distance in Å between methyl groups on opposite sides of the cavity is shown. The carbon atoms of ligand $\mathbf{L}^3$ are shown in wireframe and the hydrogen atoms are removed for clarity; distances are in Å.

red-shifted by 50 cm^{-1} in comparison with the free ligand. The general weakening of the C═O bond has been previously assigned to the increased delocalization of electron density from the now-anionic nitrogen to the amide oxygen atom.[17,31a] However, the strength of the C═O bond is sensitive to both the degree of σ-donation to the metal center (a function of the Lewis acidity of the metal which itself is dependent upon the auxiliary ligands and coordination geometry), as well as the extent of π-back-donation to the ligand. Given the complexity of factors affecting the $\nu_{C=O}$ absorption, we note that the nickel complexes **4** and **5** possess a stronger six-coordinate N_6 donor set than the zinc complex **3** which adopts a five coordinate N_3O_2 donor set, leading to a marked reduction in $\nu_{C=O}$ for both **4** and **5**. Notably, a comparison of zinc and copper complexes (vide infra), both of which contain an N_3O_2 donor set, reveal that the copper complex **6** exhibits a lower $\nu_{C=O}$ than zinc, consistent with the stronger Lewis acidity of Cu^{II} (which follows the Irving-Williams series).[31b] As expected after coordination, the IR spectrum also shows a broad band at ν = 3403 cm^{-1}, assigned to the OH str of lattice water molecules. The UV−vis spectrum of **4** in dichoromethane has three maxima at λ = 229, 262, and 331 nm respectively, assigned to $\pi-\pi^*$ and n-π^* ligand-based electronic transitions. Unfortunately, the limited solubility of the complex in the solvent precluded the observation of *d-d* transitions for this complex. FAB MS data for **4** showed only fragmentation peaks at m/z = 964, 511, and 452 assigned to $[Ni_3(\mathbf{L}^3)_2]^+$, $[Ni_2\mathbf{L}^3]^+$, and $[Ni\mathbf{L}^3]^+$ ions, respectively. Single crystals of $[Ni_3(\mathbf{L}^3)_3]$ **4** were grown via the liquid−liquid diffusion of a methanol solution of $NiCl_2{\cdot}6H_2O$ over a DCM solution of $\mathbf{L}^3H_2$ containing a few drops of Et_3N. The molecular structure of **4** was characterized by X-ray crystallography. The complex crystallizes in the trigonal space group $R\bar{3}c$, with just one-sixth of a molecule in the asymmetric unit. Each ditopic carboxamide ligand is doubly deprotonated and coordinates in a facial matter to two different Ni(II) ions to afford a neutral complex. The N_6 coordination of each Ni(II) ion is completed by a second such facially coordinated ligand. Overall, three such ligands coordinate to three octahedral Ni(II) ions, resulting in a neutral trimer. The octahedral angle distortion parameter[32a] Σ was calculated to be 98° and the mean elongation[32b] λ_{oct} = 1.027 for **4**; Σ = 118° and λ_{oct} = 1.037 for **5** (defined as $\sum = \sum_{i=1}^{12}|(90 - \theta_i)|$, where θ_i is the *cis* angles of the coordination sphere and Σ = 0 for a perfect octahedron; $\lambda_{oct} = (1/6)\sum_{i=1}^{6}(l_i/l_0)^2$, where l_i are the coordination bond lengths, l_0 is the bond length for an ideal octahedron of equivalent coordination volume and λ_{oct} = 1 for a perfect octahedron)[32] showing there is some moderate distortion in the angles around the Ni(II) ion, although the bond length variance is low. The molecular structure of **4** together with its appropriate labeling scheme is shown in Figure 7. In the copper complexes reported previously[17] the ligating atoms of $\mathbf{L}^3$ adopted a somewhat coplanar *mer*-like arrangement of the N_3 donor set; however, in the nickel complexes they produce a distinct *fac* coordination geometry with N−Ni−N angles in the range of 79.2(2)−102.4(2)°, vide infra.

Selected bond lengths and angles for **4** are summarized in Table 3; a full table of bond lengths and angles can be found in the Supporting Information (S-4). The dihedral angle between the best planes of bipyridine rings is 44°, while each terminal pyridine ring lies at an angle of 60° to the bipyridyl ring to which it is attached and by 83° to the second, more remote bipyridyl ring. The Ni(1)−N(1) and Ni(1)−N(2) bond lengths are very similar; however, the bond to the amide nitrogen N(3) is shorter by ca. 0.1 Å, consistent with its anionic N character. Due to the 3-fold axis, the intramolecular Ni(II)···Ni(II) distances are equivalent at 6.099(1) Å within the cluster. The closest intermolecular Ni(II)···Ni(II) distance is 9.175(1) Å (Figure 8). The small cavity in the center of the cluster, ca. 4.2 Å in diameter, is occupied by a single water molecule which sits on a 4-fold axis.

The trimers show a centrosymmetric set of intermolecular C−H···π and $\pi-\pi$ interactions; these are shown in Figure 9. The $\pi-\pi$ interactions occur between the pendant pyridyl

dx.doi.org/10.1021/ic501224q | Inorg. Chem. 2014, 53, 8610−8623

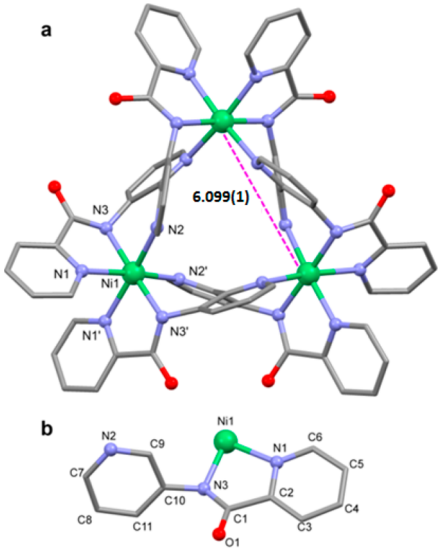

Figure 7. (a) Crystal structure of the $[Ni_3(L^3)_3]$ cluster, **4** with labels showing the relative positions of the nitrogen atoms around the metal center; (b) view of the asymmetric unit of **4** with appropriate labeling scheme. Hydrogen atoms are omitted for clarity; distances are in Å.

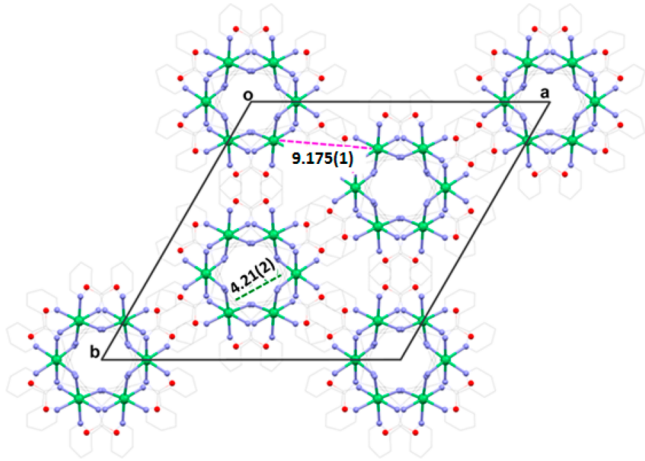

Figure 8. Packing diagram for **4**; view down the crystallographic *c*-axis showing the shortest intermolecular Ni(II)···Ni(II) distances of 9.175(1) Å (pink dashed line) and the 4.21(2) Å cavity size relative to the bipyridine backbone (green). For clarity, disordered solvent and hydrogen atoms are omitted, and the carbon atoms are shown in wireframe; distances are in Å.

groups, while the C−H···π interactions are found between the hydrogen atom at the 4-position of the pendant pyridyl ring and the aromatic system of the bipyridine backbone. This set of interactions is seen between the six neighboring molecules. The shortest intermolecular Ni(II)···Ni(II) distance (Figure 8) is found across this set of interactions. The solvent molecules participate in hydrogen bonding interactions to the carbonyl oxygen atoms of the amide group.

Interestingly, reaction of $[L^3]^{2-}$ with $Ni(OAc)_2$ afforded single crystals of a structurally very similar nickel trimer **5** whose unit cell differs from **4** as a consequence of small differences in lattice solvent (Table 4). The unit cell of **5** is notably smaller than that of **4**, by approximately 1700 Å^3. This difference is primarily along the crystallographic *c*-axes where $a = b = 23.3442(16)$ Å for **4** and 23.843(3) Å for **5**; however, $c = 24.987(4)$ Å for **4** and 20.481(7) Å for **5**. The larger amount of solvent in the lattice of **4**, and the larger MeOH molecules vs H_2O requires this larger volume, yet still yields a highly similar $[Ni_3(L^3)_3]$ triangular complex. The crystallographic data for **5** is presented in Table 1 and bond lengths and angles for the complex are presented in the Supporting Information (S-5).

It should be noted that changing the ratio of Ni(II):ligand from 2:1 to 1:1 still afforded the same Ni_3 triangular coordination complex (see Supporting Information S-6).

Previous studies of the coordination chemistry of L^3H_2 with $Cu(hfac)_2$ and $CuCl_2$ salts, afforded a dinuclear monomer and a tetranuclear dimer, respectively.[17] In the tetranuclear complex two chloride ions bridge two Cu(II) centers resulting in ferromagnetic exchange interactions between these two ions. Since acetate is a commonly used bridging ligand in the field of molecular magnetism,[33] we proposed that the use of an acetate counterion might afford a cluster or chain topology with interesting magnetic properties. Employing this strategy, reaction of one equivalent of $[L^3]^{2-}$ with two equivalents of $Cu(OAc)_2{\cdot}H_2O$ under the standard conditions described above afforded complex (**6**) as a green solid in 77% yield (Scheme 1). Single crystals suitable for single-crystal X-ray diffraction were grown via slow diffusion of diethyl ether into a 1:1 DCM/MeOH solution of **6**. The UV−vis spectrum of the complex has four absorption maxima centered at λ = 228, 256, 320, and 363 nm, assigned to $\pi-\pi^*$ and n-π^* ligand-based electronic transitions, together with a fifth weaker band at λ = 667 nm assigned to the *d-d* transitions. The FAB MS spectrum of **6** displays a parent ion at m/z = 642 for $[Cu_2L^3(OAc)_2]^+$ with

Table 3. Selected Bond Lengths and Angles for 4[a]

atoms	bond [Å]	atoms	bond [Å]
Ni(1)−N(1)	2.118(5)	Ni(1)−N(3)	2.022(4)
Ni(1)−N(2)	2.152(5)		
atoms	angle [deg]	atoms	angle [deg]
N(3)#1−Ni(1)−N(3)	178.1(3)	N(1)−Ni(1)−N(2)#1	169.9(2)
N(3)#1−Ni(1)−N(1)	79.2 (2)	N(1)#1−Ni(1)−N(2)#1	89.5(2)
N(3)−Ni(1)−N(1)	102.31(19)	N(3)#1−Ni(1)−N(2)	81.30(18)
N(3)#1−Ni(1)−N(1)#1	102.4(2)	N(3)−Ni(1)−N(2)	97.44(18)
N(3)−Ni(1)−N(1)#1	79.2(2)	N(1)−Ni(1)−N(2)	89.49(2)
N(1)−Ni(1)−N(1)#1	82.0(2)	N(1)#1−Ni(1)−N(2)	169.9(2)
N(3)#1−Ni(1)−N(2)#1	97.5(2)	N(2)#1−Ni(1)−N(2)	99.4(2)
N(3)−Ni(1)−N(2)#1	81.30(18)		

[a]Symmetry transformations used to generate equivalent atoms: #1: $x - y + 1/3, -y + 2/3, -z + 7/6$.

dx.doi.org/10.1021/ic501224q | Inorg. Chem. 2014, 53, 8610−8623

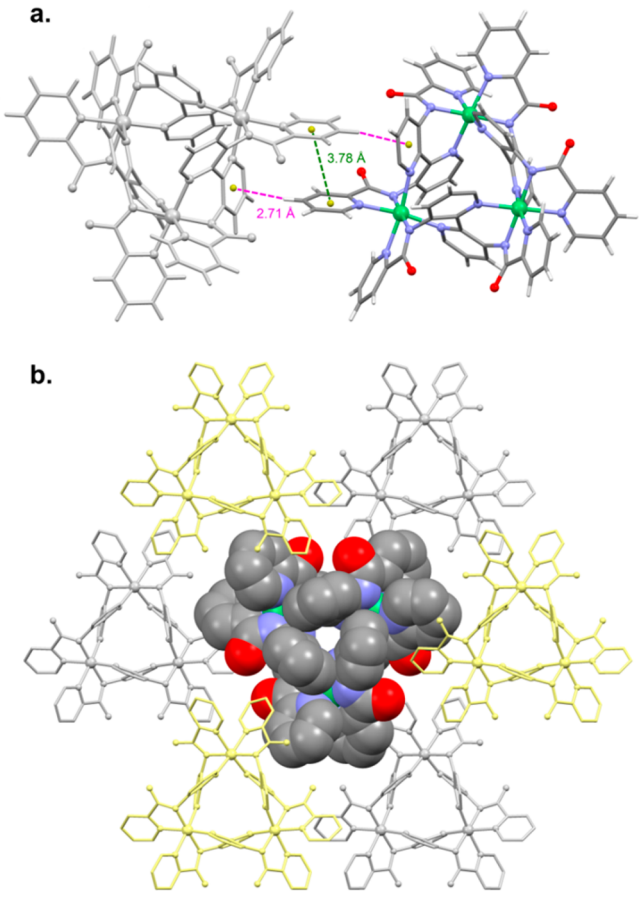

Figure 9. (a) Intertrimer $\pi\cdots\pi$ interactions (green) between pendant pyridyl groups and $^{Ar}C-H\cdots\pi$ (pink) interactions between pendant pyridyl groups and the bipy backbone; calculated centroids are shown in gold; (b) view along crystallographic *c*-axis showing nearest-neighbors. Each trimer interacts with six others, three above the plane (gold) and three below the plane of the molecule (silver).

fragmentation ions at m/z = 579 and 520 corresponding to the consecutive loss of acetate groups from the parent ion. The IR spectrum of **6** shows no N−H stretch, consistent with coordination through the anionic amide N, while a $\nu_{C=O}$ stretch is observed at 1637 cm^{-1}. Additional bands between ν = 1598−1344 cm^{-1} are assigned to acetate C−O stretches and are consistent with bidentate bridging coordination modes.[25]

The complex crystallizes in the monoclinic space group *C*2/*c*. The molecular structure of the complex is presented in Figure 10. Each crystallographically independent Cu(II) ion is bound to $[L^3]^{2-}$ in a *mer*-tridentate fashion with a chelating acetate anion, leaving a vacant coordination site available. The

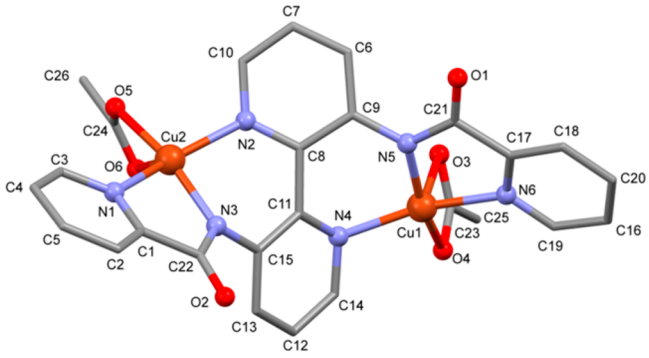

Figure 10. Molecular structure of $\{[Cu_2L^3(OAc)_2]\cdot H_2O\}_n$ **6** with the appropriate labeling scheme. Hydrogen atoms and solvent molecules are omitted for clarity.

octahedral N_3O_3 coordination sphere for Cu(2) is completed by the carboxamide O(1) of a second crystallographically equivalent unit related by an inversion center, forming a centrosymmetric dimer (Figure 11). The octahedral angle variance was calculated to be Σ = 126° for Cu(1) and Σ = 160° for Cu(2),[32a] and the mean elongation[32b] λ_{oct} = 1.139, revealing a substantially more distorted octahedron than for the nickel complex **4**.[32b] The angle variance is high, and the mean elongation is moderate which is expected for a complex undergoing Jahn−Teller distortion. The O(3) of the Cu(1) acetate additionally acts in a μ_2-bridging role to link crystallographically equivalent Cu(1) atoms related by a 2_1 screw axis (Figure 11; donor oxygen atoms labeled O(3A) and O(3B), pink). Each metal center thus has an N_3O_3 donor set and the geometry is best described as distorted octahedral; for Cu(1) the Jahn−Teller distortion is manifested in an elongation along the O(3)−Cu(1)−(O3A) axis, with a similar distortion seen for Cu(2) along the O(6)−Cu(2)−(O1′) axis (Table 5). The amide nitrogen donors N(3) and N(5) again make a bond approximately 0.1 Å shorter to the metal centers than do the pyridyl nitrogen atoms.

The torsion angle between the best planes of the bipyridine rings is 44°. The terminal pyridine rings lie at angles of 48° and 63° to the bipyridine ring to which they are directly attached, and 63° and 64° to the more remote bipyridine ring. Within the dimer units the Cu(II)···Cu(II) distances are between 6.1127(7) Å and 9.935(5) Å. The μ_2-η^2:η^1-acetate bridging between the Cu(1) atoms forms a polymeric chain structure along the crystallographic *b*-axis, with the bridging oxygen atom resulting in a short Cu(II)···Cu(II) distance of 4.6745(5) Å (Figure 12).

The chains show no significant intermolecular interactions between each other, though there are C−H···O hydrogen

Table 4. Comparison of the Two $[Ni_3(L^3)_3]$ Complexes

	4	5
formula	$[Ni_3(L^3)_3]\cdot 9CH_3OH\cdot 4H_2O$	$[Ni_3(L^3)_3]\cdot 12H_2O$
intramolecular Ni(II)···Ni(II)	6.099(1) Å	6.155(1) Å
intermolecular Ni(II)···Ni(II)	9.175(1) Å	9.066(2) Å
bipyridine dihedral angle	43.8°	40.9°
Σ (dev. from 90°)[a]	98°	108°
cavity size (bipy···bipy)	4.21(2) Å	4.184(9) Å
unit cell volume	11792 Å^3	10083 Å^3
space group	$R\bar{3}c$	$R\bar{3}c$

[a]Sum of the deviation from 90″ of the 12 *cis* angles in the coordination sphere.[32a]

dx.doi.org/10.1021/ic501224q | *Inorg. Chem.* 2014, 53, 8610−8623

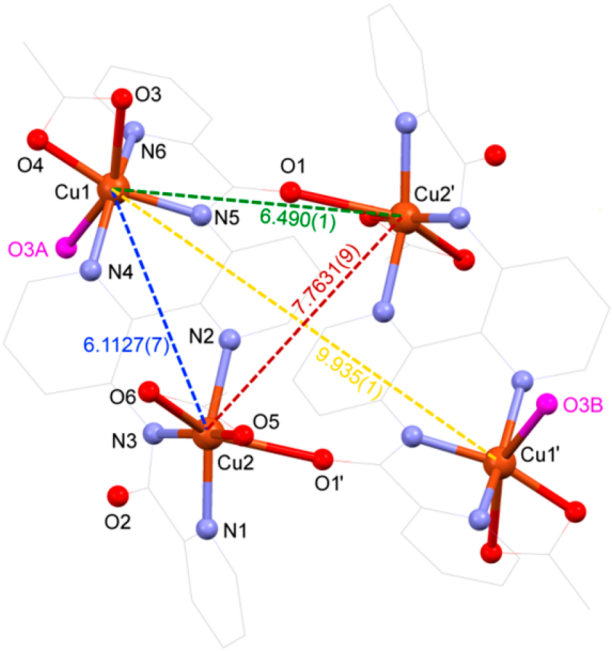

Figure 11. Molecular structure of the tetranuclear copper(II) dimer **6**, showing the intradimer Cu(II)···Cu(II) distances. Oxygen atoms coordinated to Cu(1) and Cu(1′) from adjacent dimer units are shown in pink. Carbon atoms are shown in wireframe; solvent molecules and hydrogen atoms are removed for clarity; distances are in Å. Symmetry transformations used to generate equivalent atoms: Cu1′: 1/2 − *x*, 1/2 − *y*, −*z*; Cu2′: 1/2 − *x*, 1/2 − *y*, −*z*.

bonds between the ligands and water molecules bridging the chains.

Interestingly, the molecular structure of the product formed from the coordination chemistry of $[\mathbf{L}^3]^{2-}$ with $Cu_2(OAc)_4$ is quite different from what we observed previously for the

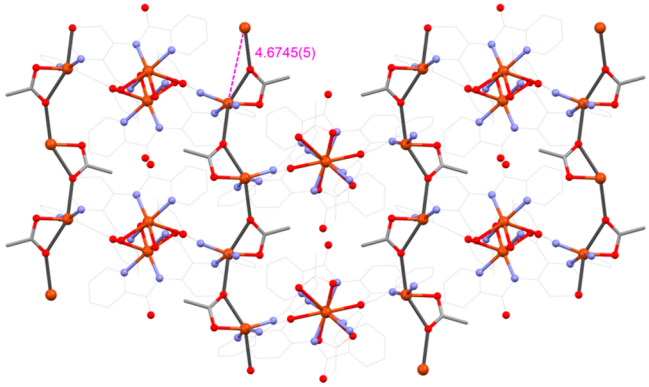

Figure 12. Crystal packing of **6** showing the acetate-bridged copper(II) ions forming a polymeric chain with the shortest Cu(II)···Cu(II) distance shown as a red dashed line. Bridging acetates are emphasized; other carbon atoms shown in wireframe and hydrogen atoms removed for clarity; distances are in Å.

$Cu(hfac)_2$ salt. In the former case, each hfac counterion coordinates in a bidentate manner to a single copper center affording a stable 6-membered chelate ring and the carbonyl groups of the amide do not participate in chelation to the Cu(II) centers facilitating the formation of a neutral, discrete complex rather than a 1-D polymer, Figure 1.

Coordination Isomers: *fac* vs *mer*. According to the work of Lippert and co-workers, the easiest way to assemble a molecular triangle is to use three 60° together with three linear fragments.[34] However, the number of reported metal-containing molecular triangles is surprisingly small.[34,35] Examples of Ni(II) triangular trimers are scarce in the chemical literature and those reported normally consist of isosceles triangles bridged by oxides with angles of 80−90°.[35a] As Ni(II) is commonly found in an octahedral coordination geometry, it

Table 5. Selected Bond Lengths and Angles for Complex 6[a]

atoms	bond [Å]	atoms	bond [Å]
Cu(1)−N(4)	2.008(1)	Cu(2)−N(1)	2.024(2)
Cu(1)−N(5)	1.927(2)	Cu(2)−N(2)	2.046(1)
Cu(1)−N(6)	2.000(1)	Cu(2)−N(3)	1.910(2)
Cu(1)−O(3)	2.448(2)	Cu(2)−O(5)	1.939(2)
Cu(1)−O(4)	1.967(2)	Cu(2)−O(6)	2.692(2)
Cu(1)−O(3)#1	2.530(2)	Cu(2)−O(1)#2	2.531(2)
atoms	angle [deg]	atoms	angle [deg]
N(5)−Cu(1)−O(4)	161.70(7)	N(3)−Cu(2)−O(5)	165.20(7)
N(5)−Cu(1)−N(6)	83.20(7)	N(3)−Cu(2)−N(1)	81.27(7)
O(4)−Cu(1)−N(6)	94.22(6)	O(5)−Cu(2)−N(1)	98.77(7)
N(5)−Cu(1)−N(4)	92.04(7)	N(3)−Cu(2)−N(2)	88.99(7)
O(4)−Cu(1)−N(4)	97.04(6)	O(5)−Cu(2)−N(2)	96.18(7)
N(6)−Cu(1)−N(4)	156.83(7)	N(1)−Cu(2)−N(2)	155.91(7)
O(3)−Cu(1)−N(4)	111.84(7)	O(6)−Cu(2)−N(4)	54.32(7)
O(3)−Cu(1)−N(5)	103.06(7)	O(6)−Cu(2)−N(5)	117.57(7)
O(3)−Cu(1)−N(6)	91.32(7)	O(6)−Cu(2)−N(6)	86.51(7)
O(3)−Cu(1)−O(4)	58.79(6)	O(6)−Cu(2)−O(4)	112.47(7)
O(3)−Cu(1)−O(3)#1	154.06(6)	O(6)−Cu(2)−O(1)#2	13519(6)
N(4)−Cu(1)−O(3)#1	81.79(7)	N(1)−Cu(2)−O(1)#2	76.10(7)
N(5)−Cu(1)−O(3)#1	98.20(7)	N(2)−Cu(2)−O(1)#2	87.33(7)
N(6)−Cu(1)−O(3)#1	76.50(7)	N(3)−Cu(2)−O(1)#2	111.74(7)
O(4)−Cu(1)−O(3)#1	98.80(6)	O(5)−Cu(2)−O(1)#2	82.41(7)

[a]Symmetry transformations used to generate equivalent atoms: #1: 1/2 − *x*, 1/2 + *y*, 1/2 − *z*. #2: 1/2 − *x*, 1/2 − *y*, −*z*.

dx.doi.org/10.1021/ic501224q | *Inorg. Chem.* 2014, 53, 8610−8623

is therefore the flexibility of the organic ligands that allows formation of the triangular structures.

In the case of the Ni(II) complexes **4** and **5**, the triangular topology is enforced by the angular geometry of the ligand. The angle between best planes of the two *fac* N_3 donor sets within each ligand moiety is calculated to be 63.5° for **4** and 63.9° for **5**, while the nickel ion behaves as the linear fragment, acting as a spacer between the two *fac* faces of its ligand environment (Figure 13). The flexibility of this ligand system therefore

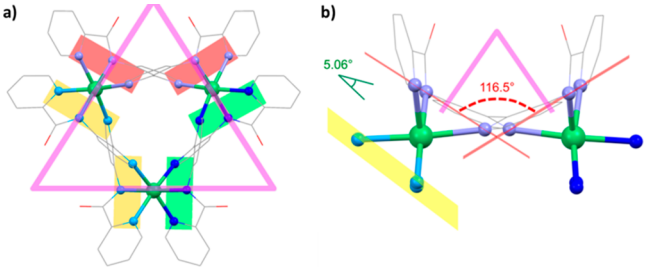

Figure 13. (a) Analysis of the triangular geometry of **4**; the Ni(II) ions behave as linear spacers between the planes formed by the approximately parallel ligand *fac* planes (red, yellow, green). (b) The 116.5° angle between the best planes of each ligand moiety coupled with the 5.1° tilt between the *fac* planes yields the angle for the triangle.

provides an excellent scaffold that can satisfy the geometrical requirements for the construction of molecular triangles; however it can also adopt both *fac* and mer geometries (for the nickel and copper complexes, respectively), as well as an intermediate geometry in the case of the zinc complex.

To explore this change in isomerism it was necessary to first be able to quantify the degree of the isomerism and hence we define an angle Φ between the best planes of the individual bidentate subunits of the N_3 donor set at the metal center (Figure 14); for ideal *mer* geometry Φ = 0°, for *fac* geometry Φ

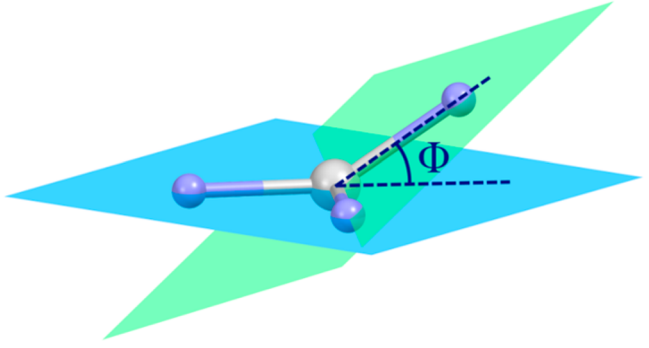

Figure 14. Definition of the Φ angle between N donors at the central metal center.

= 90°. Table 6 lists the calculated Φ values of the complexes prepared from $[\mathbf{L}^3]^{2-}$, as well as the three related complexes **6**,[36] **7**,[37] and **8**[38] with similarly constrained ligands shown in Figure 15.

As can be seen, the value for the nickel trimer (**4**) is very close to the ideal *fac* value, while the ligand in the copper chain (**6**) clearly adopts a mer conformation. The zinc dimer (**3**) can be considered midway between the two isomeric cases, although marginally toward *fac*. The previously reported Cu(II) complexes are also shown to substantially deviate from the ideal

Table 6. Φ Angle Analysis

complex/metal center	Φ [deg]	complex/metal center	Φ [deg]
(**1**)-Cu(1)[a,b]	37.7	(**6**)-Cu(2)	22.1
(**1**)-Cu(2)[a,b]	36.0	(**3**)-Zn(1)	51.0
(**1**)-Cu(3)[a,b]	37.6	(**4**)-Ni(1)	88.8
(**1**)-Cu(4)[a,b]	31.4	(**5**)-Ni(1)	86.8
(**2**)-Cu(1)[a]	35.6	(**7**)-Ni(1)[d,e]	13.7
(**2**)-Cu(2)[a]	29.0	(**7**)-Ni(1)[d,e]	15.4
(**6**)-Cu(1)[c]	27.2	(**8**)-Pd(1)[f]	8.1
(**6**)-Cu(1)	22.8		

[a]Reference 17. [b]There are two independent molecules of the $[Cu_2\mathbf{L}^3(hfac)_2]$ complex in the asymmetric unit of the complex. [c]Reference 36. [d]Reference 37. [e]The ligand moieties in complex **7** are not crystallographically equivalent. [f]Reference 38.

mer value, but this is still the best description for them. The Ni(II) and Pd(II) complexes **7** and **8** are very close to ideal mer, unsurprising for **8** due to the strong preference for palladium to adopt square planar geometries, while the Cu(II) complex **6** shows some distortion. This analysis can also be applied to the five- and six-coordinate complexes of the more flexible ligand systems in complex **9** (three complexes,[38,39] Φ = 8.9° − 10.8°) and **10** (four complexes,[40] Φ = 1.6° − 9.9°), all of which are close to the ideal mer value.

The analysis of these complexes shows that this type of N_3 ligand donor set has a noticeable preference for a mer topology. The significant difference of our Ni(II) complex from this trend caused us to rationalize this outcome further, so that future ligands can be designed for better control of the binding conformation. Figure 16 shows the torsions available for the $[\mathbf{L}^3]^{2-}$ ligand when binding to a metal ion. The values for these torsion angles are presented in Table 7.

Conjugation of the amide nitrogen with the carbonyl group results in restricted rotation around the N−CO bond; coupled with the planarity of the pyridine ring and the five-membered chelate ring that is formed, the values for ϕ_1 are small and fall within a limited range. The torsion angle between the best planes of the bipyridine rings, ϕ_3, is highly conserved across all the structures obtained, within a narrow 5° range. By far the most distinctive parameter is ϕ_2; the *mer* copper complexes have a mean value of 152.6°, to which the *fac* nickel complex shows a very large divergence. Likewise, the intermediate Zn(II) complex possesses an intermediate ϕ_2 value. In particular the ϕ_2 value for the nickel complex suggests that the amide and its attached pyridine ring should be mutually orthogonal to each other to best promote a *fac* geometry, and so we hypothesize that the introduction of additional sterically demanding groups in the 4 and 4′ positions of the bipyridine ring would promote such *fac* complexation.

Magnetic Studies of 4 and 6. The magnetic properties of single crystals of the Ni(II) trimer **4** were examined between 5 and 300 K in an applied field of 5000 Oe. Dc magnetic susceptibility data reveal that the complex obeys Curie−Weiss law with C = 4.02 $cm^3 \cdot K \cdot mol^{-1}$ and θ = +2.2 K, consistent with three S = 1 ions with g = 2.32. The positive Weiss constant indicates the presence of weak ferromagnetic interactions consistent with the absence of an efficient through-bond superexchange pathway. The value of $\chi_M T$ for the complex at 300 K is 4.02 $cm^3 \cdot K \cdot mol^{-1}$ which is close to the spin only value for three noninteracting Ni(II) ions with S = 1 and g = 2.32. Upon cooling, the data reaches a maximum of 4.91 $cm^3 \cdot K \cdot mol^{-1}$ at 11 K. The decrease in $\chi_M T$ below 11 K is attributed to

dx.doi.org/10.1021/ic501224q | Inorg. Chem. 2014, 53, 8610−8623

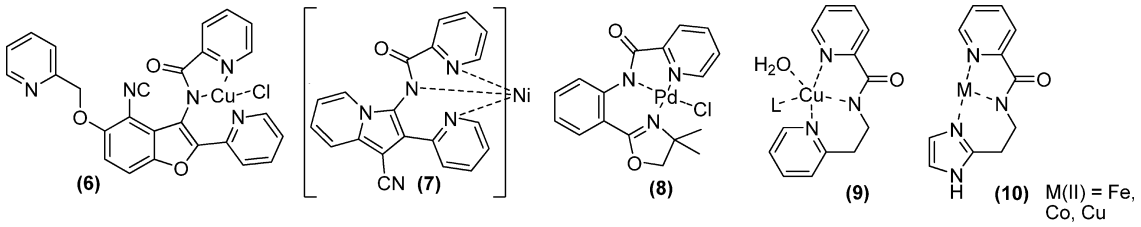

Figure 15. Similar pyridine carboxamide complexes.

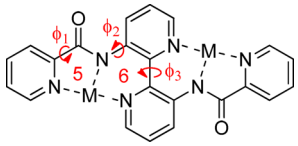

Figure 16. Torsion angles available for the tridentate binding pocket of $[L^3]^{2-}$.

Table 7. Torsion Angles of the Bipyridine Ligand $[L^3]^{2-}$

complex/metal center	ϕ [deg][a]	ϕ_1 [°][b]	ϕ_2 [°][b]	ϕ_3 [°][c]
(**4**)-Ni(1)	88.8	17(1)	96(1)	43.8
(**5**)-Ni(1)	86.8	−16.0(8)	103.3(7)	40.9
(**3**)-Zn(1)	51.0	−1.8(4)	−129.3(3)	44.8
(**1**)-Cu(1)[d]	37.7	0.2(3)	−150.6(2)	43.0
(**1**)-Cu(2)[d]	36.0	2.8(3)	−156.2(2)	43.0
(**1**)-Cu(3)[d]	37.6	0.3(2)	150.5(2)	40.6
(**1**)-Cu(4)[d]	31.4	−10.3(3)	157.9(2)	40.6
(**2**)-Cu(1)[d]	35.6	5.6(4)	−148.3(3)	42.5
(**2**)-Cu(2)[d]	29.0	2.6(4)	−164.0(3)	42.5
(**6**)-Cu(1)	22.8	11.8(3)	−149.7(2)	44.1
(**6**)-Cu(2)	22.1	8.9(3)	−143.5(2)	44.1

[a]Torsion angle between N donors at the central metal center. [b]Torsion angles for $[L^3]^{2-}$. [c]Angle calculated from best planes of the pyridine rings. [d]Reference 17.

either zero-field splitting within the ground states, Zeeman effects, or weak antiferromagnetic intermolecular interactions between the ions.

Given the high symmetry of the structure the data were modeled according to the isotropic Heisenberg−Dirac-Van-Vleck Hamiltonian for an equilateral triangle of exchange-coupled Ni(II) ions:

$$\hat{H} = -2\mathbf{J}[\hat{S}_1\hat{S}_2 + \hat{S}_2\hat{S}_3 + \hat{S}_3\hat{S}_1] \quad (1)$$

The magnetic susceptibility of an equilateral triangle of interacting $S = 1$ spins can be expressed as

$$\chi_M = \frac{2N\beta^2 g^2}{k(T-\theta)} \frac{3e^A + 10e^B + 14e^C}{1 + 9e^A + 10e^B + 7e^C} \quad (2)$$

where $A = \mathbf{J}/kT$, $B = 3\mathbf{J}/kT$ and $C = 6\mathbf{J}/kT$[41] and a mean-field term (θ) is included to take into account the effects of intertrimer antiferromagnetic exchange and/or zero-field splitting effects which are evident in the downturn in $\chi_M T$ at low temperature. A fit of the susceptibility to this expression yielded $g = 2.32$ and $\mathbf{J}/k = +4.30$ K, in reasonable agreement with Curie−Weiss behavior but required a phenomenological $\theta = -2.85$ K in order to reproduce the downturn in $\chi_M T$ at low temperature (Figure 17). The comparable magnitudes of $\mathbf{J}$ and θ indicate that the trimers are not well magnetically isolated and/or significant zero field splitting is present. Similar

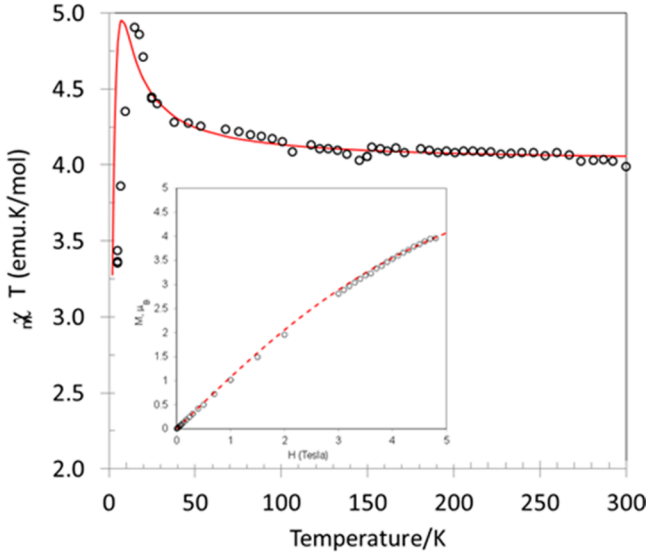

Figure 17. Plot of $\chi_M T$ vs T for complex **4**. The open circles represent the experimental data and the red line represents the best fit to a ferromagnetically coupled triangle of $S = 1$ spins (see text). Inset a fit of M vs H at 2 K to the Brillouin model for an $S_T = 3$ ground state with $g = 2.31$ ($\theta = -9$ K).

downturns in $\chi_M T$ at low temperature have been detected for other ferromagnetically coupled trimers with $S_T = 3$ ground states such as the linear Ni(II) trimer $[Ni(acac)_2]_3$, a triangulo-Ni_3-polyoxometallate[41] as well as the Schiff-base $[Ni_3]$ triangle (**12**).[46] Due to the paucity of reports of ferromagnetically coupled nickel complexes, UDFT B3LYP/LACVP**++ calculations[47] were carried out to determine the sign and strength of the exchange interaction using the approximation:

$$\mathbf{J} = -\frac{E_{HS} - E_{LS}}{\langle S^2_{HS}\rangle - \langle S^2_{LS}\rangle}$$

where E_{HS} and E_{LS} correspond to the energies of $S = 3$ and $S = 1$ configurations with corresponding expectation values $\langle S^2\rangle$. Using this approach we determined $\mathbf{J}/k = 0.80$ cm^{-1} consistent in terms of sign of $\mathbf{J}$ with the value determined from the curve-fit to the experimental data ($\mathbf{J}/k = +4.30$ K). The M vs H measurements at 2 K are consistent with an $S_T = 3$ spin system with $g = 2.32$, after taking into account a mean field correction (Figure 17, inset). Ac susceptibility measurements on **4** did not reveal any out of phase signal, indicating that it is not an SMM. As mentioned previously, examples of $[Ni_3]$ triangles are not common in the literature. A search of the Cambridge Structural Database revealed 23 hits[42] out of which there are only four reports of structurally characterized $[Ni_3]$ clusters that comprise ferromagnetically coupled Ni(II) centers giving rise to an $S = 3$ ground state, all of which are assembled from acetate[43] or the small organic ligands L^6 to L^8, Figure 18.[44−46]

dx.doi.org/10.1021/ic501224q | Inorg. Chem. 2014, 53, 8610−8623

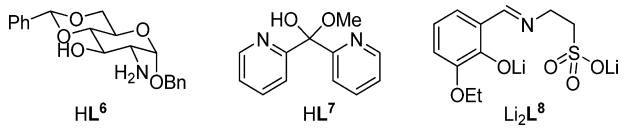

Figure 18. Small organic ligands L^6 to L^8 employed for the preparation of $[Ni_3]$ complexes **10**–**12**, respectively.[44−46]

The molecular formulas and selected magnetic parameters for these $[Ni_3]$ clusters together with complex **4** are summarized in Table 8. From this data it is clear that **4** is the first example of a ferromagnetically coupled $[Ni_3]$ triangle that has been prepared from a large, flexible polydentate ligand via solution-based chemistry. The magnetic properties of the cluster most closely resemble that of the $[Ni_3]$ Schiff-base, heterometallic cluster **12** reported by Zhang et al. in 2011,[46] however the smaller J value for **4** is consistent with the longer Ni···Ni distances due to the larger ligand.

The magnetic susceptibility of the copper complex **6** was measured in an applied field of 1000 Oe between 5 and 300 K. A plot of $1/\chi_M$ vs T (Figure 19, inset) shows that **6** obeys the Curie−Weiss law with C = 1.077 cm^3·K/mol and a negative Weiss constant θ = −6.1 K, consistent with two S = 1/2 ions with g = 2.1370 and the presence of weak antiferromagnetic interactions between the Cu(II) ions.

The g-value is typical of Cu(II) ions in which second-order spin−orbit coupling leads to $g > g_e$.[48] This value of g was confirmed by EPR measurements, Figure 20.

As previously described, the molecular structure of **6** comprises a linear chain of Cu(1) ions linked via a μ_2-acetato one-atom bridge with a Cu···Cu distance, associated with the acetate-bridged chain of 4.67 Å (Figure 13). The second crystallographically independent Cu(II) center is linked to the chain. The remaining through-bond interactions comprise a three atom O−C−N bridge via the carboxamide linking Cu(1) and Cu(2′) at 6.1127(7) Å and via the four atom N−C−C−N unit of the 2,2′-bipyridine backbone linking Cu(1) and Cu(2) at 6.490(1) Å (Figure 12). The large internuclear distances and multiple-atom bridges suggested that the best magnetic model is therefore a one-dimensional chain of interacting Cu(1) ions and a series of isolated Cu(2) ions. A fit of the magnetic susceptibility to the Heisenberg linear chain[49] with an additional term accounting for a noninteracting Cu(II) center (eq 3 afforded g = 2.40 and J/k = −11 K and reproduced the data well, down to ca. 7 K. At these low temperatures weaker exchange between chains or between Cu(1) and Cu(2) centers likely become significant.

$$\chi = \frac{Ng^2\beta^2}{kT}\frac{(0.25 + 0.14995x + 0.30094x^2)}{(1 + 1.9862x + 0.68854x^2 + 6.0626x^3)} + \frac{Ng^2\beta^2 S(S+1)}{3kT} \quad (3)$$

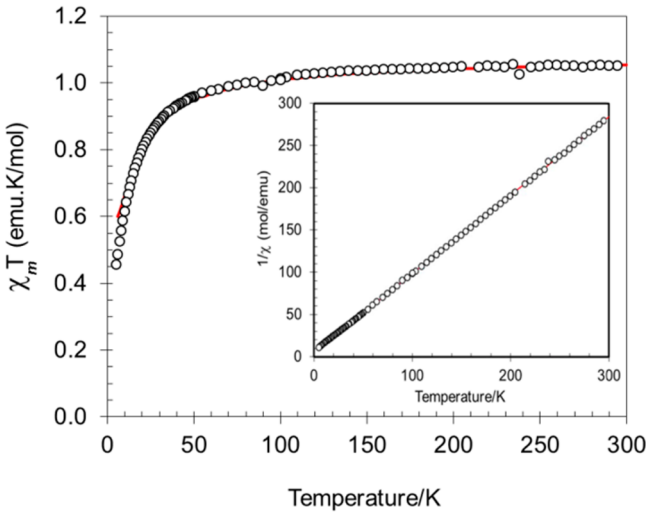

Figure 19. Plot of $\chi_M T$ vs T for complex **6**. Open circles represent the experimental data and the solid red line represents the fit to a linear chain of S = 1/2 spins (g = 2.40, J/k = −11 K) with an equal number of non-interacting S = 1/2 ions. Inset: Curie−Weiss behavior for **6**.

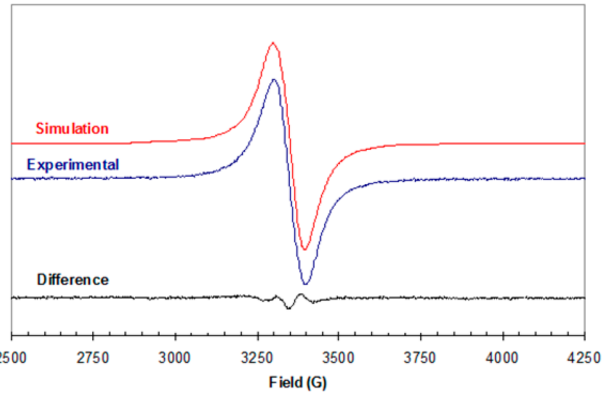

Figure 20. Observed and simulated EPR spectra for **6**. Simulation parameters were $g_{\|}$ = 2.1370, $g_{\perp}$ = 2.0905 using line widths of 56 G (parallel) and 62 G (perpendicular) and a Lorentzian line shape.

where $x = J/kT$.

The weakness of the antiferromagnetic interactions can be explained by the fact that the one-atom bridge lies along the Jahn−Teller distortion axis and hence has minimal overlap with the anticipated $d_{x^2-y^2}$ magnetic orbital (based on simple crystal field splitting under Jahn−Teller elongation).

CONCLUSION

To summarize, we have demonstrated that the 3,3′-di-(picolinamolyl)-2,2′-bipyridine ligand L^3 can react with a variety of first row transition metal ions yielding a number of

Table 8. Molecular Formulas and Selected Magnetic Parameters for Ferromagnetic $[Ni_3]$ Triangular Complexes with S = 3

complex	J (cm^{-1})	g	S	ref
$[Ni_3(OAc)_3(N_3)_3(py)_5]$ (**9**)	+15.7, −1.2	2.16	3	43
$[Ni_3(L^6)_5(HL^6)]NO_3$ (**10**)	+16.4, +11.0	2.183	3	44
		2.247		
$[Ni_3(L^7)_4]I_2$·2.5MeOH (**11**)	+12.5, −0.5	2.13	3	45
$[Ni_3Li(L^7)_3(OH)(CH_3CN)_3]0.5CH_3CN$ (**12**)	+4.27	2.31	3	46
$[Ni_3(L^3)_3]$·6H_2O (**4**)	+2.99	2.32	3	This work

dx.doi.org/10.1021/ic501224q | Inorg. Chem. 2014, 53, 8610−8623

coordination topologies. In addition to the previously reported dinuclear monomer and tetranuclear dimer structures,[17] a second tetranuclear dimer, a [Ni_3] triangle, and a 1-D Cu(II) chain have been isolated. The ligand has yielded complexes which exhibit *fac* and *mer* isomers, with the *fac* isomer yielding an isolated trimeric cluster topology. An analysis of the ligand from the crystallographic data has been undertaken, and a rationale for the modification of this system to favor such coordination has been proposed that should promote the formation of molecular triangles or higher dimensional structural topologies. The magnetic properties of the [Ni_3] triangle are particularly interesting in that the three Ni(II) centers are ferromagnetically coupled giving rise to an $S = 3$ ground state and as such it joins the small family of four other structurally characterized Ni(II) triangles displaying this type of magnetic behavior. This study demonstrates that rational design strategies can be employed alongside serendipitous approaches to prepare coordination complexes with diverse structural topologies and interesting magnetic properties.

■ ASSOCIATED CONTENT

Ⓢ Supporting Information

Tables of bond lengths and angles for the ligand $\mathbf{L}^3H_2$ and complexes **3**−**6**, additional experimental data, and a Curie−Weiss plot for **4**. This material is available free of charge via the Internet at http://pubs.acs.org.

■ AUTHOR INFORMATION

Corresponding Author

*E-mail: mpilkington@brocku.ca. Tel: +1 905 688 5550, ext. 3403.

Notes

The authors declare no competing financial interest.

■ ACKNOWLEDGMENTS

This work was supported by MRI ERA (M.P.), NSERC (D.G., M.P., and J.M.R.), CRC (M.P. and J.M.R.), Brock University, CFI (New Opportunities, M.P.) and OIT (matching funds, M.P.). We are indebted to Mr. Tim Jones for provision of mass spectral data and to Prof. Art van der Est and Mr Sam Mula for the EPR spectrum of complex **6**. We also thank Prof. F.S. Razavi for access to the SQUID magnetometer at Brock University.

■ REFERENCES

(1) *Supramolecular Chemistry: From Molecules to Nanomaterials*; Steed, J. W.; Gale, P. A., Eds.; Wiley: New York, 2012.

(2) (a) Beauty in Chemistry: Artistry in the Creation of New Molecules. Fabbrizzi, L., Ed.; *Topics in Current Chemistry*; Springer: New York, 2013; Vol. *323*, p 1. (b) Chambron, J.-C.; Sauvage, J.-P. *New J. Chem.* **2013**, *37*, 49. (c) Forgan, R. S.; Sauvage, J.-P.; Stoddart, J. F. *Chem. Rev.* **2011**, *111*, 5434. For some recent examples see: (d) Gillissen, M. A. J.; Koenigs, M. M. E.; Spiering, J. J. H.; Vekemans, J. A. J. M.; Palmans, A. R. A.; Voets, I. K.; Meijer, E. W. *J. Am. Chem. Soc.* **2014**, *136*, 336. (e) Castilla, A. M.; Ramsay, W. J.; Nitschke, J. R. *Chem. Lett.* **2014**, *43*, 256. (g) Ramsay, W. J.; Ronson, T. K.; Clegg J. K.;. (f) Nitschke, J. R. *Angew. Chem., Int. Ed.* **2013**, *52*, 13439. Stephenson, A.; Ward, M. D. *Dalton Trans.* **2011**, *40*, 10360.

(3) (a) *Transition Metals in Supramolecular Chemistry*; Sauvage, J. P., Ed.; Wiley: New York, 1999. (b) *Transition Metals in Supramolecular Chemistry*; Fabbrizzi, L., Poggi, A., Eds.; Springer: New York, 1995. (c) Saalfrank, R. W.; Maid, H.; Scheurer, A. *Angew. Chem., Int. Ed.* **2008**, *47*, 8794. (d) Pilkington, M.; Decurtins, S. In *Crystal Engineering in Materials Chemistry*; Desiraju, G., Ed.; Wiley-VCH: Weinheim, Germany, 2003; p 276. (e) Pilkington, M.; Gross, M.; Franz, P.; Biner, M.; Decurtins, S.; Stoeckli-Evans, H.; Neels, A. *J. Solid State Chem.* **2001**, *159*, 262.

(4) (a) Smith, A. P.; Fraser, C. L. In *Comprehensive Coordination Chemistry II, Vol. 1*; McCleverty, J. A., Meyer, T. J., Eds.; Pergamon Press: New York, 2003; pp 1−23. (b) *Chemistry of Heterocyclic Compounds, Vol. 14: Pyridine Metal Complexes*; Tomasik, P., Ratajewicz, Z., Newkome, G. R., Strekowski, L., Eds.; John Wiley & Sons: New York, 1985. (c) Constable, E. C.; Steel, P. J. *Coord. Chem. Rev.* **1989**, *93*, 205. (d) Summers, L. A. *Adv. Heterocycl. Chem.* **1984**, *35*, 281. (e) Newkome, G. R.; Patri, A. K.; Holder, E.; Schubert, U. S. *Eur. J. Org. Chem.* **2004**, 235.

(5) (a) Fletcher, N. C. *J. Chem. Soc., Perkin Trans. 1* **2002**, 1831. (b) Chelucci, G.; Tummel, R. P. *Chem. Rev.* **2002**, *102*, 3129.

(6) (a) Juris, A.; Balzani, V.; Barigelletti, F.; Campagna, S.; Belser, P.; von Zelewsky, A. *Coord. Chem. Rev.* **1988**, *84*, 85. (b) Le Bozec, H.; Renouard, T. *Eur. J. Inorg. Chem.* **2000**, *2*, 229.

(7) (a) Schubert, U. S.; Eschbaumer, C. *Angew. Chem., Int. Ed.* **2002**, *41*, 2892. (b) Decurtins, S.; Schmalle, H. W.; Zheng, L.-M.; Ensling, J. *Inorg. Chim. Acta* **1996**, *244*, 165. (c) Gorp, J. J. V.; Vekemans, J. J. A. M.; Meijer, E. W. *J. Am. Chem. Soc.* **2002**, *124*, 14759.

(8) (a) Connor, J. A.; Wallis, J. D.; Baxter, P. N. W.; Povey, D. C.; Powell, A. K. *Polyhedron* **1992**, *11*, 1771. (b) Nocton, G.; Booth, C. H.; Maron, L.; Andersen, R. A. *Organometallics* **2013**, *32*, 5305. (c) Murray, P. R.; Crawford, S.; Dawson, A.; Delf, A.; Findlay, C.; Jack, L.; McInnes, E. J. L.; al-Musharafi, S.; Nichol, G. S.; Oswald, I.; Yellowlees, L. J. *Dalton Trans.* **2012**, *41*, 201. (d) Shan, B.-Z.; Zhao, Q.; Goswami, N.; Eichhorn, D. M.; Rillema, D. P. *Coord. Chem. Rev.* **2001**, *211*, 117. Menon, S.; Rajesekharan, M. V.; Tuchagues, J.-P. *Inorg. Chem.* **1997**, *36*, 4341. (e) Geary, E. A. M.; Yellowlees, L. J.; Jack, L. A.; Oswald, I. D. H.; Parsons, S.; Hirata, N.; Durrant, J. R.; Robertson, N. *Inorg. Chem.* **2005**, *44*, 242. (f) Cargill Thompson, A. M. W.; Jeffrey, J. C.; Liard, D. J.; Ward, M. D. *J. Chem. Soc., Dalton Trans.* **1996**, 879. (g) Hasegawa, Y.; Hieda, R.; Miyata, K.; Nakagawa, T.; Kawai, T. *Eur. J. Inorg. Chem.* **2011**, *32*, 4978.

(9) Rice, C. R.; Onions, S.; Vidal, N.; Wallis, J. D.; Senna, M.-C.; Pilkington, M.; Stoeckli-Evans, H. *Eur. J. Inorg. Chem.* **2002**, *8*, 1985.

(10) (a) Cargill Thompson, A. M. W.; Jeffery, J. C.; Liard, D. J.; Ward, M. D. *J. Chem. Soc., Dalton Trans.* **1996**, 879. (b) Boyle, T. J.; Ottley, L. A. M.; Rodriguez, M. A. *Polyhedron* **2008**, *27*, 3079.

(11) (a) Tong, M.-L.; Yang, G.; Chen, X.-M. *Aust. J. Chem.* **2000**, *53*, 607. (b) Huang, X.-C.; Zhang, L.-Y.; Chen, X.-M.; Ng, S. W. *Acta Crystallogr.* **2004**, *E60*, m332.

(12) Transition metal complexes: (a) Zhang, X.-M.; Wu, H.-S.; Chen, X.-M. *Eur. J. Inorg. Chem.* **2003**, 2959. (b) Wei, M.; Wang, X.; Duan, X. *Chem.—Eur. J.* **2013**, *19*, 1607. Lanthanide complexes: (c) Ji, B.; Deng, D.; He, X.; Liu, B.; Miao, S.; Ma, N.; Wang, W.; Ji, L.; Liu, P.; Li, X. *Inorg. Chem.* **2012**, *51*, 2170. (d) Mingyan, W.; Feilong, J.; Youfu, Z.; Rui, F.; Lian, C.; Maochun, H. *Inorg. Chem. Commun.* **2012**, *15*, 25.

(13) (a) Hu, M.; Wang, Q.-I.; Xu, G.-F.; Deng, G.-R.; Yang, G.-M.; Yu, M.; Zhang, Y.-H. *Inorg. Chim. Acta* **2007**, *360*, 1684. (b) Chen, X.-L.; Yao, Y.-J.; Hu, H.-M.; Chen, S.-H.; Fu, F.; Han, Z.-X.; Qing, T.; Yang, M.-L.; Xue, G.-L. *Inorg. Chim. Acta* **2009**, *362*, 2686.

(14) (a) Belda, O.; Moberg, C. *Coord. Chem. Rev.* **2005**, *249*, 727. (b) Rajput, A.; Mukherjee, R. *Coord. Chem. Rev.* **2013**, *257*, 350.

(15) Patra, A. K.; Mukherjee, R. *Inorg. Chem.* **1999**, *38*, 1388.

(16) Wang, J.; Onions, S.; Pilkington, M.; Stoeckli-Evans, H.; Halfpenny, J. C.; Wallis, J. D. *Chem. Commun.* **2007**, 3628.

(17) Wang, J.; Djukic, B.; Cao, J.; Alberola, A.; Razavi, F. S.; Pilkington, M. *Inorg. Chem.* **2007**, *46*, 8560.

(18) (a) Wang, J.; Slater, B.; Alberola, A.; Stoeckli-Evans, H.; Razavi, F. S.; Pilkington, M. *Inorg. Chem.* **2007**, *46*, 4763. (b) Zarrabi, N.; Hayward, J. J.; Clegg, W.; Pilkington, M. *Dalton Trans.* **2014**, 2352.

(19) *APEX-II*; Bruker AXS Inc.: Madison, WI.

(20) *SADABS*; Bruker AXS Inc.: Madison, WI.

(21) Sheldrick, G. M. *Acta Crystallogr.* **2008**, *A64*, 112.

(22) (a) Spek, A. L. *J. Appl. Crystallogr.* **2003**, *36*, 7. (b) Spek, A. L. *Acta Crystallogr.* **2009**, *D65*, 148. (c) van der Sluis, P.; Spek, A. L. *Acta Crystallogr.* **1990**, *A46*, 194.
(23) Rawson, J. M. *PIP4WIN* v. 1.2; University of Windsor: Windsor, ON, 2011.
(24) *Jaguar* version 8.0; Schrödinger LLC: New York, NY, 2013.
(25) Ditchfield, R.; Hehre, W. J.; Pople, J. A. *J. Chem. Phys.* **1971**, *54*, 724.
(26) (a) Hay, P. J.; Wadt, W. R. *J. Chem. Phys.* **1985**, *82*, 270. (b) Wadt, W. R.; Hay, P. J. *J. Chem. Phys.* **1985**, *82*, 284. (c) Hay, P. J.; Wadt, W. R. *J. Chem. Phys.* **1985**, *82*, 299.
(27) Lee, C.; Yang, W.; Parr, R. G. *Phys. Rev. B* **1988**, *37*, 785.
(28) (a) Hunter, C. A.; Sanders, J. K. M. *J. Am. Chem. Soc.* **1990**, *112*, 5525. (b) Wright, J. D. *Molecular Crystals*, 2nd ed., Cambridge University Press: Cambridge U.K., 1995.
(29) Kumar, U.; Thomas, J.; Thirupathi, N. *Inorg. Chem.* **2010**, *49*, 62.
(30) Addison, A. W.; Rao, T. N.; Reedijk, J.; van Rijn, J.; Verschoor, G. C. *J. Chem. Soc., Dalton Trans.* **1984**, 1349.
(31) (a) Jain, S. L.; Bhattacharyya, P.; Milton, H. L.; Slawin, A. M. Z.; Crayston, J. A.; Woollins, J. D. *J. Chem. Soc., Dalton Trans.* **2004**, 862. (b) Houghton, R. P. *Metal complexes in organic chemistry*; Cambridge University Press: Cambridge, U.K., 1979.
(32) (a) Drew, M. G. B.; Harding, C. J.; McKee, V.; Morgan, G. G.; Nelson, J. *J. Chem. Soc., Chem. Commun.* **1995**, 1035. (b) Robinson, K.; Gibbs, G. V.; Ribbe, P. H. *Science* **1971**, *172*, 567. Fleet, M. E. *Mineral. Mag.* **1976**, *40*, 531.
(33) Aubin, S. M. J.; Wemple, M. W.; Adams, D. M.; Tsai, H.-L.; Christou, G.; Hendrickson, D. N. *J. Am. Chem. Soc.* **1996**, *118*, 7746.
(34) Schnebeck, R.-D.; Freisinger, E.; Glahé, F.; Lippert, B. *J. Am. Chem. Soc.* **2000**, *122*, 1381.
(35) (a) Dong, G.; Chun-ying, D.; Chen-jie, F.; Qing-jin, M. *J. Chem. Soc., Dalton Trans.* **2002**, 834. (b) Esteban, J.; Ruiz, E.; Font-Bardia, M.; Calvet, T.; Escuer, A. *Chem.—Eur. J.* **2012**, *18*, 3637. (c) Efthymiou, C. G.; Raptopoulu, C. P.; Terzis, A.; Perlepes, S. P.; Escuer, A.; Papatriantafyllopoulou, C. *Polyhedron* **2010**, *29*, 627.
(36) Kan, W. Q.; Xia, D.-C.; Ma, J.-F. Z. *Kristallogr.-New Cryst. Struct.* **2010**, *225*, 97.
(37) Niyomura, O.; Yamaguchi, Y.; Sakao, R.; Minoura, M.; Okamoto, Y. *Heterocycles* **2008**, *75*, 297.
(38) Decken, A.; Gossage, R. A.; Yadav, P. N. *Can. J. Chem.* **2005**, *83*, 1185.
(39) Wu, C.-Y.; Su, C.-C. *Polyhedron* **1997**, *16*, 2465.
(40) (a) Brown, S. J.; Tao, X.; Stephan, D. W.; Mascharak, P. K. *Inorg. Chem.* **1986**, *25*, 3377. (b) Tao, X.; Stephan, D. W.; Mascharak, P. K. *Inorg. Chem.* **1987**, *26*, 754. (c) Delany, K.; Arora, S. K.; Mascharak, P. K. *Inorg. Chem.* **1988**, *27*, 705. (d) Brown, S. J.; Tao, X.; Wark, T. A.; Stephan, D. W.; Mascharak, P. K. *Inorg. Chem.* **1988**, *27*, 1581.
(41) (a) Ginsberg, A. P.; Martin, R. L.; Sherwood, R. C. *Chem. Commun.* **1967**, 856. (b) C. J. Gomez-Garcia, C. J.; Coronado, E.; Ouahab, L. *Angew. Chem., Int. Ed.* **1992**, *31*, 649.
(42) Canaj, A. B.; Nodaraki, L. E.; Philippidis, A.; Tzimopoulus, D. I.; Fotopoulou, E.; Siczek, M.; Lis, T.; Milios, C. J. *RSC Adv.* **2013**, *3*, 13214.
(43) Milios, J. C.; Prescimone, A.; Sanchez-Benitez, J.; Parsons, S.; Murrie, M.; Brechin, E. K. *Inorg. Chem.* **2006**, *45*, 7053.
(44) Burkhardt, A.; Speilberg, E. T.; Simon, S.; Gorls, H.; Buchholz, A.; Pass, W. *Chem.—Eur. J.* **2009**, *15*, 1261.
(45) Katsenis, A. D.; Kessler, V. D.; Papaefstathiou, G. S. *Dalton Trans.* **2011**, *40*, 4590.
(46) Chen, F.-Y.; Zhang, S. H.; Li, P. H.; Zhang, L. J.; Zhang, Y. D. *J. Mol. Struct.* **2011**, *1006*, 142.
(47) (a) Gómez-Coca, S.; Ruiz, E. *Dalton Trans.* **2012**, *41*, 2659. (b) Kalaban, L.; Matar, S. F.; Desplanches, C.; Létard, J. F.; Zakhour, M. *Chem. Phys.* **2008**, *352*, 85.
(48) (a) Song, J.-L.; Dong, Z.-C.; Zeng, H.-Y.; Zhou, W.-B.; Naka, T.; Wei, Q.; Mao, J.-G.; Guo, G.-C.; Huang, J.-S. *Inorg. Chem.* **2003**, *42*, 2136. (b) Abragam, A.; Bleaney, B. *Electron Paramagnetic Resonance of Transition Ions*; Oxford University Press: New York, 1970.
(49) Tucker, D. A.; White, P. S.; Trojan, K. L.; Kirk, M. L.; Hatfield, W. E. *Inorg. Chem.* **1991**, *30*, 823.